Eur. Phys. J. C (2023) 83:821
https://doi.org/10.1140/epjc/s10052-023-11910-3

THE EUROPEAN PHYSICAL JOURNAL C

Regular Article - Theoretical Physics

Possible existence of traversable wormhole in Finsler–Randers geometry

Krishna Pada Das[a], **Ujjal Debnath**[b]

Department of Mathematics, Indian Institute of Engineering Science and Technology, Shibpur, Howrah 711 103, India

Received: 24 June 2023 / Accepted: 5 August 2023

Abstract In the present article, we have explored the possible existence of a traversable wormhole in the framework of Finsler–Randers (F–R) geometry. In order to achieve this goal, first, we have constructed gravitational field equations for static, spherically symmetric spacetime with anisotropic fluid distribution in F–R geometry. Next, we have written the deduced form of field equations in the background of Morris–Thorne wormhole geometry. To visualize the shape of the wormhole, we have selected exponential shape function $b(r) = \frac{r}{exp\left(\eta\left(\frac{r}{r_0}-1\right)\right)}$ with the constant parameter η and the throat radius r_0 and depicted two-dimensional and three-dimensional embedding diagrams corresponding to some considered values of η and r_0. Moreover, all essential requirements to build a wormhole shape have been examined for the reported shape function. Next, We have analyzed wormhole configuration for three cases (I, II, III) corresponding to three selected redshift functions. Furthermore, each case is analyzed by dividing it into two models such as (i) *Model-1* (for general anisotropic EoS $p_t = \chi p_r$) and (ii) *Model-2* (for linear phantom-like EoS $p_r + \omega\rho = 0$). In each model of three cases, we have verified the validity of the wormhole solution in F–R geometry by considering null, weak, strong and dominant energy conditions. Also, the total amount of averaged NEC-violating matter near the wormhole throat has been analyzed by computing volume integral quantifier.

1 Introduction

In modern cosmology, based on several observational tests, it has been observed that our current universe is in an expansion phase in an accelerating way [1–6]. As a responsible candidate, the so-called dark energy (DE) plays the main role behind this expansion. In GR [7], Einstein connects the Riemannian geometry to gravitation by a system of equations known as Einstein's field equations. However, till today, GR faces some problems regarding DE and direct exploration of the current expanding universe. For this purpose, to perform these problems, several DE models and modified theories of gravities (MTG) have already been established [8–11]. In the recent few years, various results from observable astrophysical studies it has been shown that an anisotropic direction of expansion of the universe may happen if the underlying geometry is anisotropic. In this connection, a new interesting alternative gravitational theory was established on generalized Riemannian geometry known as Finslerian geometry. The most fundamental distinction of Finsler's geometry is that it incorporates the concept of anisotropic intrinsically in the geometry of spacetime. The underlying space of Finsler's geometry is named Finsler space, a metric space. The metric in this space is defined as a function $F(x, y)$ from a tangent bundle of a manifold to $\mathbb{R}^1$. Here $F(x, y)$ is a non-negative function, mathematically defined as the norm instead of the inner product on a tangent bundle with the position of spacetime coordinate x and a tangent vector $y \in T_xM$ representing the velocity. Hence the Finslerian geometry is dynamic geometry depending on position and direction, i.e., dynamical coordinates on a tangent bundle of a differentiable manifold, whereas the Riemannian geometry is gravitational geometry. In the framework of this type of geometry, several researchers have studied different cosmological aspects [12–20].

Now Finsler–Randers spacetime, originated by Randers, is a special type of Finsler spacetime that govern by a generalized Riemannian metric as

$$F(x, y) = \sqrt{g_{ij}y^i y^j} + A_\lambda y^\lambda. \tag{1}$$

The physical significance of this metric describes as the additional extra term $A_\lambda y^\lambda$ considered as the minimum cause of

[a] e-mail: krishnapada0019@gmail.com (corresponding author)
[b] e-mail: ujjaldebnath@gmail.com

Published online: 14 September 2023

relativity violation, or deviation from isotropic to anisotropic nature of spacetime, or violation of Lorentz symmetry. The F–R spacetime gives a special interest to the investigation of the Riemannian model/FRW model in a generalized Riemannian spacetime because the introduction of vector field affects the geometrical terms like curvature, metric and geodesics and also acts as a dark energy fluid. There are a lot of research works for the FRW metric that have already investigated F–R spacetime successfully. Now, we want to focus on a brief review of several research works regarding cosmological and geometrical aspects in the following.

In Ref. [15], authors have first constructed gravitational field equations in Randers-type metric corresponding to FRW metric and studied several cosmological aspects, including the Finslerian Raychaudhuri equation. The Lorentz invariance violation and symmetries of Finsler–Randers space have been studied in detail in Ref. [21]. A comparative study between the F–R model and the DGP model has been done in detail and concluded these two models are almost cosmological equivalent [22]. Finsler–Randers cosmology can imitative a general dark energy scenario and also modified gravity model, shown in the Ref. [23]. F–R cosmological model corresponding to modified gravity has been studied in [18], and also authors discussed all energy conditions in this framework in detail. The extended Schwarzschild-like and Schwarzschild De-Sitter solutions in Finsler–Randers geometry and its geometrical applications have been explored by constructing geodesic paths of a particle and as well as a comparison study between GR and S–F–R framework [24,25]. Also, from the dynamical system perspective, F–R cosmological model and its outstanding applications are included in Ref. [26]. Dynamical analysis of several geometrical aspects like geodesic, angular momentum, the energy of a moving particle, deflection angle etc., is discussed in the Refs. [27–29]. Based on the F–R metric, authors studied differential geometry with remarkable applications, and also the Raychaudhuri equation, as well as energy conditions, are discussed in detail in the Refs. [30,31].

Due to the strong gravitational field, it was considered that the physical structure of the end status of a static, massive astrophysical object should be spherically symmetric. In this connection, the interior spacetime of a compact object, or compact star, is assumed as spherically symmetric spacetime. Here, for example, a compact object or star may be a black hole, a white dwarf, or a neutron star to a strange star etc. After the discovery of a new and appropriate approach to gravitational theory based on the concept of curvature of spacetime, known as Einstein's General theory of relativity (GR) [7], the investigation of numerous exact solutions of interior and exterior geometry become a new platform of research in the scientific community till today. For this purpose, the spherically symmetric spacetime that is able to explore astrophysical phenomena regarding physical characteristics and impact of compact objects has always achieved one of the most interesting problems in particle astrophysics.

Now among compact relativistic objects, a more interesting and ideological object (i.e., mathematically possible but without observational evidence) is a wormhole. From the physical point of view, a wormhole is described as a tunnel-like structure that connects two different points of spacetime or two points of two different spacetimes. Historically, the notion of the wormhole was actually initiated by Flamm [32] soon after the invention of the Schwarzschild solution [33]. The idea of these hypothetical shortcuts was first proposed by Einstein and Rosen, popularly known as the Einstein–Rosen bridge, in order to investigate the co-ordinate or curvature singularity free for the Riessner-Nordstron solution [34,35] and the Schwarzschild solution [36]. In a seminal work in 1962, Wheeler [37] first used the term wormhole and describe the geometry of Schwarzschild wormhole and later Hawking [38] transformed this solution into Euclidean wormhole, named as Einstein–Rosen bridge. After some years, it is investigated by Wheeler and Fuller [39] that the Einstein–Rosen bridge type of wormhole may not be stable because when it connects two parts of the same universe, it will pinch off very quickly than light or any particle moving slower than light is not able to fall in from one exterior region to make it to the other exterior region.

The idea of the static and spherically symmetric traversable wormhole was first successfully explored by Morris and Thorne [40] as a possible structure to freely traverse time or interstellar. The intention of time or interstellar travel was able to explain by imposing a special type of matter near the throat that must push the wormhole wall apart and prevents it from squeezing very quickly from gravitational collapse. Hence, the fundamental constituents near the throat of a traversable wormhole must be the exotic matter that violates the null energy condition (NEC), at least in the neighbourhood of the throat. Thus in order to construct a traversable wormhole configuration, the main issue is the violation of energy conditions that claim the presence of exotic matter near the throat of wormhole [41–44]. Moreover, Visser et al. [41,45] revealed an important essential fact that the averaged null energy condition (ANEC) must be violated in the wormhole geometry, and the measurement of this type matter should be infinitesimally small, named as the volume integral quantifier. Till today, there are a lot of research works regarding physical aspects and as well as exact solutions for different types of wormholes such as static wormhole [46–50], dynamical wormhole [51,52] and rotating wormholes [53,54] have already been developed by several authors. Consequently, a lot of research works are done by assuming the wormhole configuration supported by several types of dark energy such as cosmological constant [55–57], phantom energy [58–60], modified or generalized Chaplygin gas [61–63]. Besides GR, a large number of wormhole models

are developed in the framework of different modified theories of gravities (MTGs). Here an interesting fact is that in the context of MTGs for the construction of wormholes, the exotic matter can be minimized or completely avoided. Again except the Riemannian geometry, wormhole configuration has already been studied by several researchers in the background of different geometrical gravitational theories like Teleparallel geometry, non-commutative geometry and Finslerian geometry etc. Among these geometrical, we want to concentrate on wormhole structure in Finslerian geometry because of some interesting special consequences in this geometry. First of all, Riemannian geometry is a special type of Finslerian geometry, and it is dynamic, already stated in detail in the early stage of this section [64]. Now the exact solution of traversable wormhole in the Finslerian framework was first successfully studied by Rahaman et al., [65] by constructing some redshift functions and shape functions with the help of EoS. Recently, a wormhole solution in Finsler geometry with $f(R,T)$ gravity has been explored in the Refs. [66,67]. Also, traversable wormhole supported by Phantom-like dark energy in the framework of Finslerian geometry has been discussed by Singh et al. [68].

In the present study, our main goal is to construct gravitational field equations in the context of Finsler–Randers geometry. For this purpose, we consider a static metric to describe a spherically symmetric spacetime geometry with an anisotropic fluid distribution. Next, our aim is to examine the formation of Morris and Thorne [40] traversable wormhole in F–R geometry. For this context, we are employing two EoS to evaluate Rander terms such as general anisotropic EoS, discussed in the *Model-1* and phantom-like EoS, discussed in the *Model-2*. A brief decoration of the rest portion of the whole study is as follows: In the Sect. 2, we have included a details construction of gravitational field equations in the F–R geometry corresponding to a static, spherically symmetric spacetime. Next, the formation of Morris and Thorne wormhole configuration has been discussed in the Sect. 3. In this section, we have included a discussion of several aspects like embedding surface, proper radial distance, the validity of energy conditions etc., regarding wormhole configuration. Further, in Sect. 4, we have analyzed averaged NEC for our wormhole solutions. At the end section, i.e., Sect. 5, we have reported some valuable conclusions from our whole discussions.

2 Gravitational field equations for F–R metric

A Finsler space is governed by a differentiable function $F(x,y)$, also named as Finsler structure, defined on a tangent bundle TM of a manifold M as

$$F(x,y): TM \to \mathbb{R}$$

The function satisfies some following properties:

(i) F is smooth on $T\tilde{M} = TM \setminus \{0\}$, regularity property.
(ii) F is a positive one dimensional homogeneous function $F(x,\lambda y) = \lambda F(x,y)$ with $\lambda > 0$, homogeneity property, where $x \in M$ and $y = \frac{dx}{d\tau}$ are the respective representation of position and velocity.
(iii) The $n \times n$ Hessian matrix [64]

$$g_{\mu\nu} \equiv \left(\frac{1}{2}F^2\right)_{y^\mu y^\nu} \tag{2}$$

is positive-definite at every point of $TM \setminus \{0\}$, referred as strong convexity property, where the notation $()_{y^\mu} \equiv \frac{\partial}{\partial y^\mu}()$.

A special type of Finsler space the so-named the Finsler–Randers space [69], defined by the metric function of the form as

$$F(x,y) = \alpha(x,y) + \beta(x,y), \tag{3}$$

where

$$\alpha(x,y) = \sqrt{g_{ij}y^i y^j}, \tag{4}$$

$$\beta(x,y) = u_\lambda y^\lambda, \tag{5}$$

and $g_{ij}(x)$ is the fundamental metric tensor corresponding to Riemannian affine connection. Hence as a consequence, we can say that the geometrical structure of F–R space is obviously a generalization of Riemannian geometry.

Here the spatial coordinates are comoving the time coordinate describes the proper time surveyed by the comoving observer. The vector field $y^\mu = \frac{dx^\mu}{ds}$ describes the four tangent vectors that represent the velocity of a comoving observer towards a suitable family of world lines (i.e., paths of fluid flow) in a locally anisotropic universe. The arclength $s \equiv$ is the proper time. So we have $y^\mu = (1,0,0,0)$.

u_λ represents a weak primordial vector field with $|u_\lambda| \ll 1$ and $u_\lambda = (u_0,0,0,0)$ with $u_0(r)$. Here u_λ is a covector. Now using the Hessian of F, the metric for the Finslerian spacetime can be defined as follows:

$$f_{\mu\nu}(x,y) = \frac{1}{2}\frac{\partial^2 F^2}{\partial y^\mu \partial y^\nu}(x,y). \tag{6}$$

By simplifying we can derive [15,24] in the following form

$$f_{\mu\nu} = a_{\mu\nu} + \frac{1}{4\alpha}(u_\mu y_\nu + u_\nu y_\mu) - \frac{\beta}{\alpha^3}y_\mu y_\nu + u_\mu u_\nu \tag{7}$$

where

$$a_{\mu\nu}(x,y) = \frac{F}{\alpha}(x,y)g_{\mu\nu}(x). \tag{8}$$

With respect to the metric of Finslerian spacetime the usual definition of Christoffel symbols are as follows

$$\Gamma^i_{jk}(x,y) = \frac{1}{2} f^{ir}(x,y) \left[f_{rj,k}(x,y) + f_{rk,j}(x,y) - f_{jk,r}(x,y)\right]. \tag{9}$$

And the corresponding Cartan tensor defined by E. Cartan as

$$C_{ijk} = \frac{1}{2}\left(\frac{\partial f_{ij}}{\partial y^k}\right). \tag{10}$$

Here it is important to mention that the tensor quantity C_{ijk} plays the role of the torsion tensor in the Finslerian geometrical framework. Thus a Finsler space becomes a Riemannian space when $C_{ijk} = 0$ and vice-versa.

Now, the osculating Riemannian metric can be defined for the case of a connection between a convenient Finsler metric and Riemannian metric as [14,70]

$$r_{\mu\nu}(x) = f_{\mu\nu}(x, y(x)). \tag{11}$$

The corresponding Christoffel symbols are

$$r^k_{\lambda\mu}(x) = \Gamma^k_{\lambda\mu}(x,y) + C^k_{\mu\rho}(x,y)\frac{\partial y^\rho}{\partial x^\lambda}(x) + C^k_{\lambda\rho}(x,y)\frac{\partial y^\rho}{\partial x^\mu}(x) - a^{k\sigma}(x,y)C_{\lambda\mu\rho}(x,y)\frac{\partial y^\rho}{\partial x^\sigma}(x). \tag{12}$$

The full expression of Cartan's torsion tensor can be easily defined as [71]

$$C_{\mu\nu\lambda} = \frac{1}{2}\Big[\frac{1}{\alpha}\mathcal{S}_{(\mu\nu\lambda)}(g_{\mu\nu}u_\lambda) - \frac{1}{\alpha^3}\mathcal{S}_{\mu\nu\lambda}(y_\mu y_\nu u_\lambda) - \frac{\beta}{\alpha^3}\mathcal{S}_{\mu\nu\lambda}(g_{\mu\nu}y_\lambda)\Big]. \tag{13}$$

All term of the above equation is proportional to the the field u_λ thus $C_{\mu\nu\lambda} \approx 0$. So the approximation form of Christoffel components are

$$A^k_{\lambda\nu}(x) \approx \Gamma^k_{\lambda\nu}(x). \tag{14}$$

The curvature tensor can be defined as

$$L^k_{\lambda\mu\nu} = A^k_{\lambda\nu,\mu} - A^k_{\lambda\mu,\nu} + A^\rho_{\lambda\nu}A^k_{\rho\mu} - A^\rho_{\lambda\mu}A^k_{\rho\nu}. \tag{15}$$

Ricci tensor

$$L_{\mu\nu} = L^\kappa_{\mu\kappa\nu}. \tag{16}$$

Scalar curvature

$$L = f^{\mu\nu}L_{\mu\nu}. \tag{17}$$

Let us considered a static spherically symmetric metric as

$$ds^2 = e^\zeta dt^2 - e^\psi dr^2 - r^2\left(d\theta^2 + sin^2\theta d\phi^2\right), \tag{18}$$

where ζ and ψ are arbitrary functions of radial coordinate r only.

So we have

$$g_{ij}(x) = diag\left(e^\zeta, -e^\psi, -r^2, -r^2 sin^2\theta\right) \tag{19}$$

Utilizing the Eq. (7), we can easily compute the following relations between Finslerian ($f_{\mu\nu}$) and Riemannian ($g_{\mu\nu}$) metric coefficients with $\{\mu, \nu = 0, 1, 2, 3\}$.

$$\left.\begin{aligned} f_{00} &= g_{00} + \frac{u_0 g_{00}}{2\sqrt{g_{00}}} + u_0^2 \\ f_{11} &= g_{11}\left(1 + \frac{u_0}{\sqrt{g_{00}}}\right) \\ f_{22} &= g_{22}\left(1 + \frac{u_0}{\sqrt{g_{00}}}\right) \\ f_{33} &= g_{33}\left(1 + \frac{u_0}{\sqrt{g_{00}}}\right) \end{aligned}\right\} \tag{20}$$

Now, by imposing the conditions $u_0'' \approx 0$ and $u_0'^2 \approx 0$ and putting the metric coefficients g_{ij}, given in the Eq. (19), the nonzero components of Ricci tensor ($L_{\mu\nu}$, defined in the Eq. (15)) can evaluated as follows:

$$L_{00} = \frac{e^{-\psi}}{8r}\Big[e^{\zeta/2}u_0'\left(4 + r(2\zeta' - \psi')\right) + 2e^\zeta\left(\zeta'\left(4 + r(\zeta' - \psi')\right) + 2r\zeta''\right)\Big], \tag{21}$$

$$L_{11} = \frac{1}{8r}\Big[8\psi' + e^{-\zeta/2}u_0'\left(-8 + 5r(2\zeta' + \psi')\right) - 2r\left(\zeta'^2 - \zeta'\psi' + 2\zeta''\right)\Big], \tag{22}$$

$$L_{22} = \frac{e^{-\psi}}{8}\Big[-8 + 8e^\psi - 4r(\zeta' - \psi') + 2re^{-\zeta/2}u_0'\left(-7 + r(\zeta' + \psi')\right)\Big]. \tag{23}$$

$$L_{33} = \sin^2\theta L_{22}. \tag{24}$$

Now the energy–momentum tensor for describing Finslerian anisotropic matter distribution can be given for a comoving obserever as

$$T_{\mu\nu}(x,y) = (\rho + p_t)y_\mu y_\nu - p_t f_{\mu\nu}(x,y) + (p_r - p_t)z_\mu z_\nu, \tag{25}$$

where y_μ are fluid 4-velocity vector and z_μ are radial 4-vector. So the components of $T_{\mu\nu}$ can given as follows

$$\left.\begin{aligned} T_{00} &= \rho f_{00} \\ T_{11} &= -p_r f_{11} \\ T_{22} &= -p_t f_{22} \\ T_{33} &= -p_t f_{33} \end{aligned}\right\} \tag{26}$$

The trace is

$$T = \rho - p_r - 2p_t. \tag{27}$$

Based on the Asanov research [14], the action for the osculating Riemannian spacetime can be defined as

$$I = \int L(x, y(x))\sqrt{-g(x, y(x))}\, d^4x, \tag{28}$$

where $\boldsymbol{L(x, y(x))}$ is the osculating Ricci scalar in the context of Finslerian geometry.

Now using the variational principle for the above action (28), the field equations of Einstein's GR corresponding to our model can be written as follows

$$L_{\mu\nu} = 8\pi G\Big(T_{\mu\nu} - \frac{1}{2}T g_{\mu\nu}\Big). \tag{29}$$

So the componentwise field equations can be written as

$$\begin{aligned} &e^{-\zeta-\psi}\Big[e^{\zeta/2}u_0'\big(4 + r(2\zeta' - \psi')\big) \\ &\quad + 2e^{\zeta}\big(\zeta'(4 + r(\zeta' - \psi')) + 2r\zeta''\big)\Big] \\ &\quad = 32\pi G r(\rho + p_r + 2p_t), \end{aligned} \tag{30}$$

$$\begin{aligned} &e^{-\psi}\Big[8\psi' + e^{-\zeta/2}u_0'\big(-8 + 5r(2\zeta' + \psi')\big) \\ &\quad - 2r\big(\zeta'^2 - \zeta'\psi' + 2\zeta''\big)\Big] = 32\pi G r(\rho + p_r - 2p_t), \end{aligned} \tag{31}$$

$$\begin{aligned} &\frac{e^{-\psi}}{r}\Big[-8 + 8e^{\psi} - 4r(\zeta' - \psi') \\ &\quad + 2re^{-\zeta/2}u_0'\big(-7 + r(\zeta' + \psi')\big)\Big] \\ &\quad = 32\pi G r(\rho - p_r). \end{aligned} \tag{32}$$

Solving the above field Eqs. (30)–(32), the explicit expressions of ρ, p_r and p_t can be evaluated as follows:

$$\rho(r) = \frac{e^{-\psi}\left(u_0' e^{-\frac{\zeta}{2}} r\left(2r\zeta' + r\psi' - 4\right) + 2r\psi' + 2e^{\psi} - 2\right)}{16\pi G r^2}, \tag{33}$$

$$p_r(r) = \frac{e^{-\frac{\zeta}{2}-\psi}\left(r\zeta'\left(u_0' r + 2e^{\zeta/2}\right) + 3u_0' r - 2e^{\zeta/2}\left(e^{\psi} - 1\right)\right)}{16\pi G r^2}, \tag{34}$$

$$p_t(r) = \frac{e^{-\frac{\zeta}{2}-\psi}\left(u_0'\left(-4r\zeta' - 5r\psi' + 2r\psi' + 6\right) + 2e^{\zeta/2}\left(2r\zeta'' + \left(\zeta' - \psi'\right)\left(r\zeta' + 2\right)\right)\right)}{64\pi G r}. \tag{35}$$

3 Wormhole model

In this section, our goal is to examine the formation of a traversable wormhole in the context of F–R geometry. For this purpose, we first recall a brief review of traversable wormholes based on the Morris and Thorne proposition for wormhole description. To represent such type wormhole geometry, first, we consider the following static, spherically symmetric line element [40]

$$ds^2 = e^{2\Phi(r)}dt^2 - \frac{dr^2}{1 - \frac{b(r)}{r}} - r^2\big(d\theta^2 + \sin^2\theta d\phi^2\big), \tag{36}$$

where, $\Phi(r)$ and $b(r)$ are the gravitational redshift function and the shape function, respectively.

Now from the physical point of view, to depict the hypothesised picture of a wormhole by the metric (36), the function $b(r)$ should be in a form such that it connects two asymptotically flat regions of spacetime. Here the minimum value attained by $b(r)$ is called the throat of the wormhole. As the function $b(r)$ depicts the shape of the wormhole, it is named by the shape function.

According to Morris and Thorne, a traversable wormhole with r_0 as the radius of the throat will be depicted by the metric (36), then the shape function must maintain the following restrictions

- Throat condition: $b(r_0) = r_0$ and $1 - \frac{b(r)}{r} > 0$ for $r > r_0$.
- Flaring out condition: $b'(r_0) < 1$ at $r = r_0$.
- Asymptotically flatness condition: $\frac{b(r)}{r} \to 0$ for $r \to \infty$.

Motivated from the valuable research works on Cosmological model done by several authors [15,16,18,22,23,26,27,71] in F–R geometry, we have defined the Morris–Thorne wormhole metric in the context of F–R geometry, defined by the metric (3) i.e., may be named by Morris–Thorne–Finsler–Randers metric as

$$F(x, y) = \sqrt{g_{ij}y^i y^j} + u_\lambda y^\lambda, \tag{37}$$

where

$$g_{ij}(x) = \mathrm{diag}\left[e^{2\Phi(r)}, -\frac{1}{1 - \frac{b(r)}{r}}, -r^2, -r^2\sin^2\theta\right]. \tag{38}$$

In the 'Appendix', we have reported a details discussion regarding the computation of field equations corresponding to the metric (37).

Now, the field equations (30)–(32) for the metric (37) reduce to the following forms

$$\rho(r) = \frac{e^{-\Phi(r)}\left(b'(r)\left(u_0' r + 2e^{\Phi(r)}\right) + u_0' b(r)\left(3 - 4r\Phi'(r)\right) + 4u_0' r\left(r\Phi'(r) - 1\right)\right)}{16\pi G r^2}, \tag{39}$$

$$p_r(r) = \frac{\left(1 - \frac{b(r)}{r}\right)e^{-\Phi(r)}\left(-\frac{2b(r)e^{\Phi(r)}}{r - b(r)} + 2r\left(u_0' r + 2e^{\Phi(r)}\right)\Phi'(r) + 3u_0' r\right)}{16\pi G r^2}, \tag{40}$$

$$p_t(r) = \frac{1}{64\pi G r}\left(\left(1 - \frac{b(r)}{r}\right)e^{-\Phi(r)}\left(2e^{\Phi(r)}\left(\frac{\left(2r\Phi'(r) + 2\right)\left(-rb'(r) + 2r(r - b(r))\Phi'(r) + b(r)\right)}{r(r - b(r))} + 4r\Phi''(r)\right)\right.\right.$$
$$\left.\left. - \frac{u_0'\left(r\left(3b'(r) + 8r\Phi'(r) - 6\right) + b(r)\left(3 - 8r\Phi'(r)\right)\right)}{r - b(r)}\right)\right). \tag{41}$$

In the present work, let us choose the shape function $b(r)$ in the following form

$$b(r) = \frac{r}{exp\left(\eta\left(\frac{r}{r_0} - 1\right)\right)}, \tag{42}$$

where η ia a constant parameters and r_0 is the radius of wormhole throat. Next, in order to scrutinize the essential requirements of a wormhole shape function, several plots have been drawn for some considered values of η in Fig. 1 corresponding $r_0 = 1$ and Fig. 2 corresponding to $r_0 = 2$. From these Figures, it is observed that throat condition, flaring out condition, and asymptotically flatness condition are fulfilled by our considered shape function $b(r)$ with chosen values of η and r_0.

3.1 Embedding surface

For a better visualization of the wormhole geometry, presented by Eq. (36), we have illustrated embedded two-dimensional and three-dimensional diagrams for the shape function, stated in Eq. (42). Since our wormhole geometry is spherically symmetric, we have used an equatorial slice, represented by $\theta = \frac{\pi}{2}$, and fixed a moment of time by t =constant, without loss of generality. We have presented this type of hypersurface by $H : \theta = \pi/2, t =$ constant and hence in this hypersurface, $d\theta = 0$ and $dt = 0$. So, for this connection, we may write the reduced form of the wormhole metric (36) as

$$ds_H^2 = -\frac{dr^2}{1 - \frac{b(r)}{r}} - r^2 d\phi^2. \tag{43}$$

In the cylindrical co-ordinates the above metric (43) equivalent to the following form

$$ds_H^2 = -dZ^2 - dr^2 - r^2 d\phi^2. \tag{44}$$

Now, in three-dimensional Euclidean space the embedding surface characterize by $Z = Z(r)$, so, the reduced form of the metric for this surface may be written as [72]

$$ds_H^2 = -\left[1 + \left(\frac{dZ}{dr}\right)^2\right]dr^2 - r^2 d\phi^2. \tag{45}$$

Now comparing the Eqs. (43) and (44), we can represent the embedding shape function $Z(r)$ as follows

$$\frac{dZ}{dr} = \pm\sqrt{\left(1 - \frac{b(r)}{r}\right)^{-1} - 1}. \tag{46}$$

Utilizing the Eq. (46), we have depicted embedded 2D diagram in Fig. 3 and embedded 3D diagram in Fig. 4.

3.2 Proper radial distance

In the proper radial co-ordinate system, the wormhole metric (36) can be written as [72,73]

$$ds^2 = e^{2\Phi(l)}dt^2 - dl^2 - r(l)^2\left(d\theta^2 + \sin^2\theta d\phi^2\right). \tag{47}$$

Now the proper radial distance of the wormhole is given by

$$l(r) = \pm\int_{r_0}^{r}\left(1 - \frac{b(r)}{r}\right)^{-\frac{1}{2}}dr, \tag{48}$$

where the '$\pm$' comes for the both mouths of wormhole.

In Fig. 5, we have illustrated the proper radial distance while the radial coordinate $r \geq r_0$. Moreover, in Tables 1 and 2, we have calculated the approximate numerical values of proper radial distance $l(r)$ and embedding surface function $Z(r)$ of the wormhole for the first quadrant at several radial coordinate $r \geq r_0^+$. And it is observed that the values of $l(r)$ are slightly more than $Z(r)$ at any radial coordinate r.

3.3 Energy conditions

The energy conditions are defined by a set of inequalities among the thermodynamical parameters like ρ, p_r, p_t. These conditions originated from Raychaudhuri equations, which represent the action of congruence and the attractive nature of

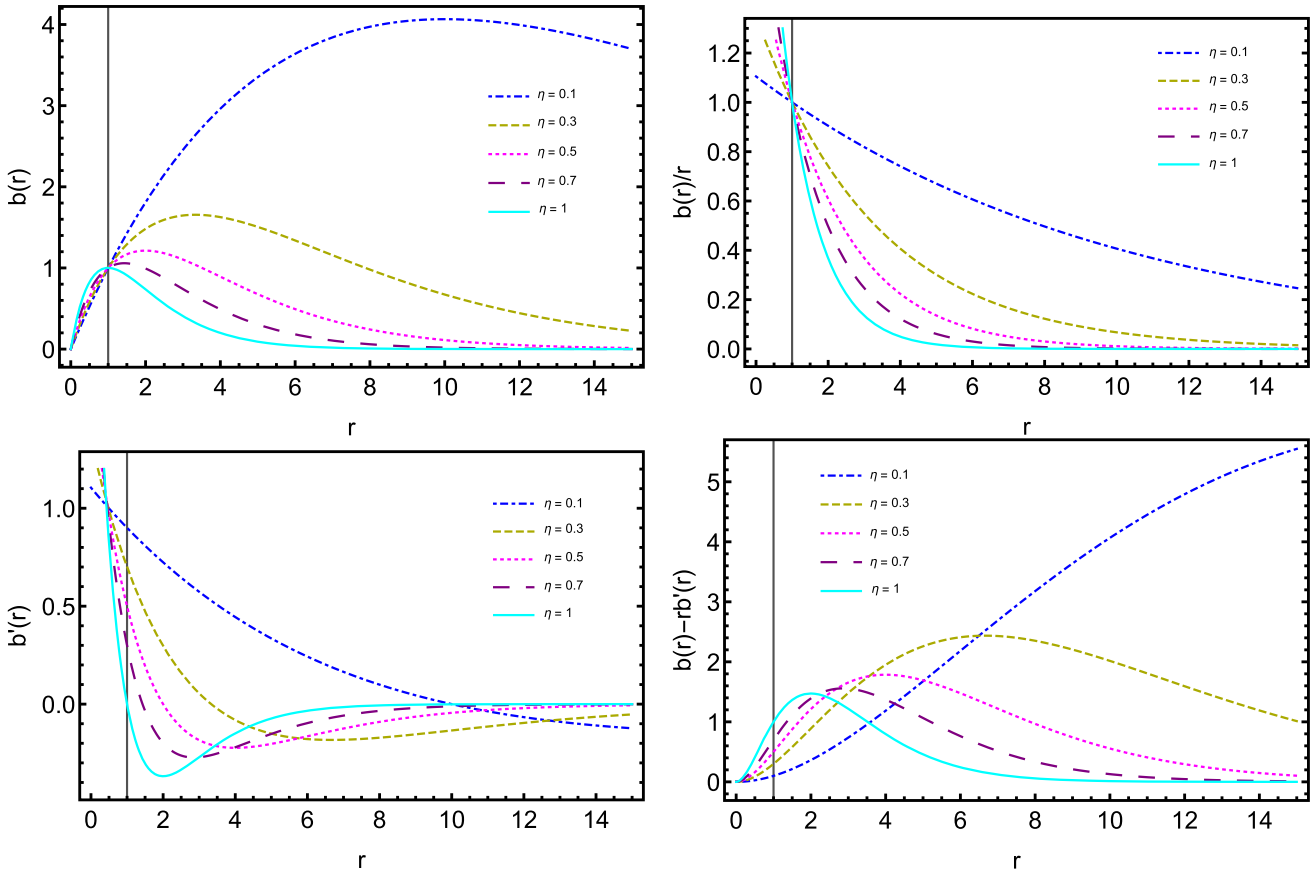

Fig. 1 Behavior of b, $\frac{b}{r}$, b', $b - rb'$ against the radial coordinate r with $r_0 = 1$

gravity for timelike, spacelike, or lightlike curves [74]. The energy conditions are mainly used as the fundamental tools to predict the nature of a strong gravitational field because the geodesic structure of spacetime may be described perfectly by these conditions. Moreover, one can analyze the realisticness of matter distribution and hence the possible existence of wormhole geometry by utilizing these conditions. An interesting fact is that the energy conditions are purely geometrical concepts, and their origin is not dependent on the theory of gravity (for more details, see the Ref. [75]). Here we will emphasize only four distinct kinds of energy conditions, whereas, in GR, seven different types of energy conditions are analyzed [76]. Since the whole of our current discussion is performed with anisotropic fluid, the energy conditions are given as follows:

- NEC (Null energy condition): $\rho + p_r \geq 0$, $\rho + p_t \geq 0$. In tensor form NEC is defined as $T_{\mu\nu}k^\mu k^\nu \geq 0$ with null-like vector k^μ.
- WEC (Weak energy condition): $\rho \geq 0$, $\rho + p_r \geq 0$, $\rho + p_t \geq 0$. In tensor form WEC defined as $T_{\mu\nu}U^\mu U^\nu \geq 0$ with time-like vector U^μ.
- SEC (Strong energy condition): $\rho + p_r \geq 0$, $\rho + p_t \geq 0$, $\rho + p_r + 2p_t \geq 0$. In tensor form SEC defined as $\left(T_{\mu\nu} - \frac{T}{2}g_{\mu\nu}\right)U^\mu U^\nu \geq 0$ with the trace of the energy–momentum tensor $T_{\mu\nu}$ i.e., $T = \rho - \Sigma_i p_i$.
- DEC (Dominant energy condition): $\rho \geq 0$, $\rho - |p_r| \geq 0$, $\rho - |p_t| \geq 0$. In tensor form DEC defined as $T_{\mu\nu}U^\mu U^\nu \geq 0$ and $T_{\mu\nu}U^\mu$ is not space-like.

Now, the physical meaning of the above energy conditions i.e., NEC, WEC, SEC and DEC may be described as follows:

(i) The WEC implies the observer's measurements along any time-like vector about energy density (ρ) must be always positive i.e., $\rho \geq 0$.
(ii) The SEC implies that the gravitational field should always attractive i.e., may predict a strong gravitational field.
(iii) DEC states that the measurements of energy flux by any observer is time-like or null-like and must be always non-negative i.e., $\rho \geq 0$.
(iv) The basic requirements of SEC and WEC is NEC i.e., WEC $\subset$ NEC and SEC $\subset$ NEC.

Therefore, if the NEC is hold then the SEC and WEC are automatically hold but the reverse need not always true. Again we have DEC $\subset$ WEC $\subset$ NEC and hence we can say DEC implies both the NEC and the WEC, while the reverse doesn't

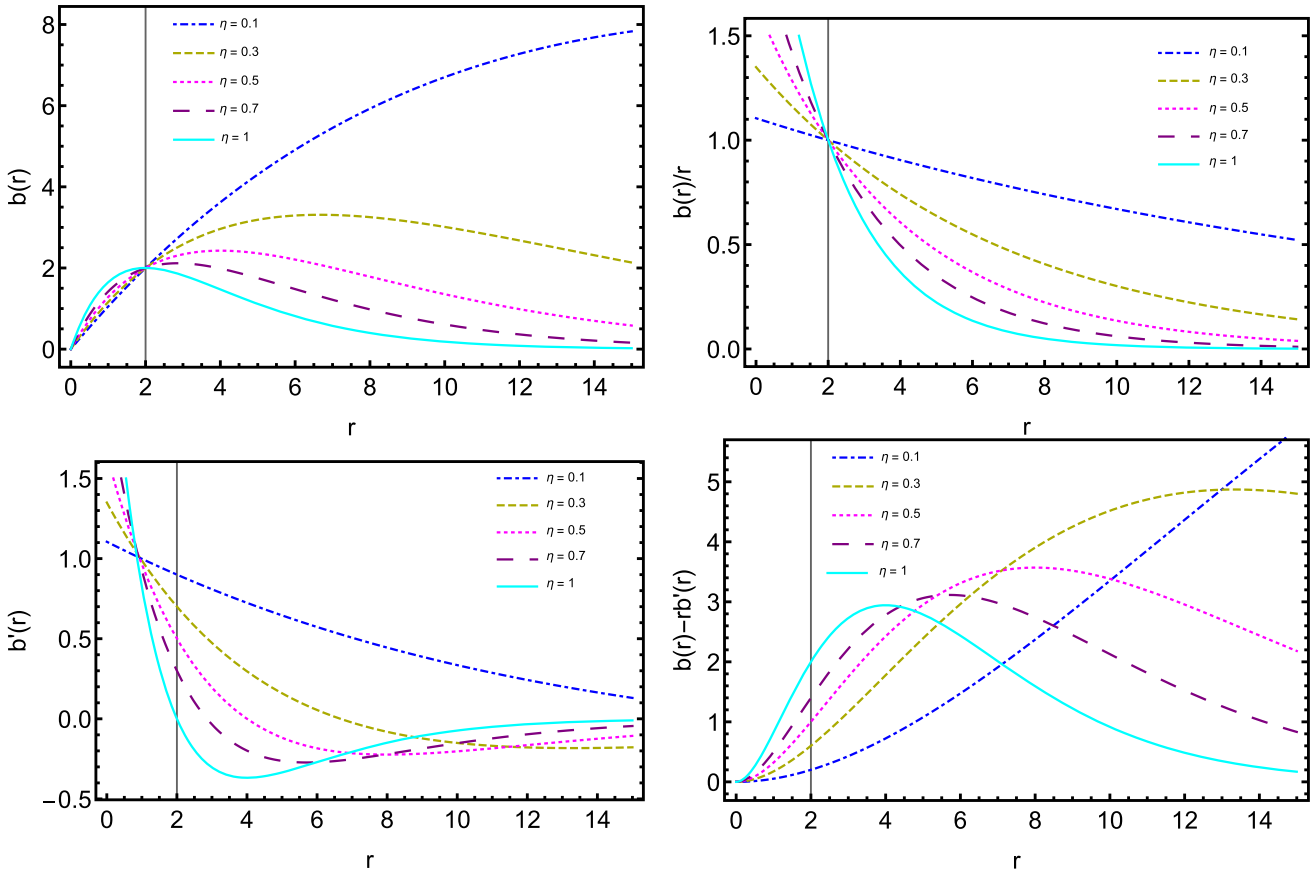

Fig. 2 Behavior of b, $\frac{b}{r}$, b', $b - rb'$ against the radial coordinate r with $r_0 = 2$

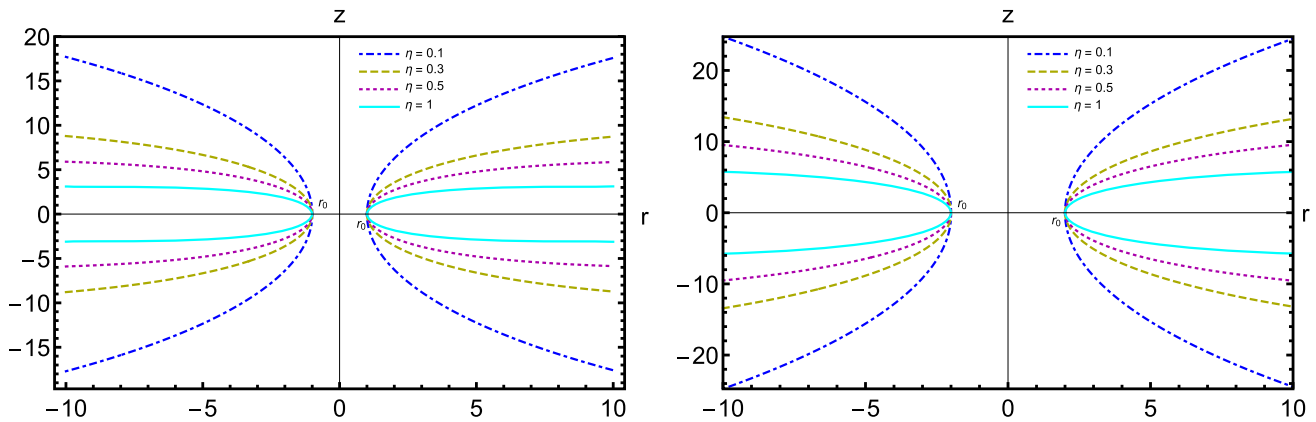

Fig. 3 Embedding two-dimensional diagram plots corresponding to the relation (46) with the shape function (42) for the throat radius $r_0 = 1$ (left panel) and $r_0 = 2$ (right panel)

need to be true in each case. Moreover, DEC need not imply the SEC. Now, a basic aspect of traversable wormhole i.e., wormhole with the exotic matter violates NEC in the context of GR [41]. Also, in order to describe a wormhole geometry the violation of SEC is necessary. Thus again if the NEC is violated then all other standard energy conditions are also violated.

By a bouncing Universe, we may treat a Universe that undergoes a collapse, attain a minimum and later on expands [77–81]. In classical cosmology, it has been observed that such bounce may not be possible for FRW universe if $\rho + 3p > 0$ i.e. active mass is positive with perfect fluid's energy density ρ and pressure p [82]. Thus, FRW Universe undegoing a bounce with minimum at which the SEC must be violated. However, the violation of SEC is necessary but not sufficient condition. In the early Universe, some bouncing models may be produced based on the violation of WEC [79]. Again, the violation of WEC is also a necessary condition

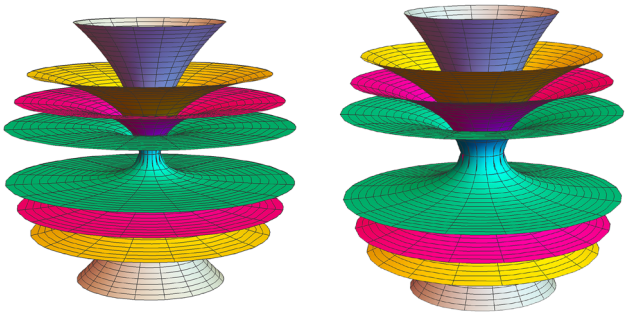

Fig. 4 Embedding three-dimensional diagram plots corresponding to the relation (46) with the shape function (42) for the throat radius $r_0 = 1$ (left panel) and $r_0 = 2$ (right panel). Here the colors indicated as $\eta = 0.1 \rightarrow$ ♠, $\eta = 0.3 \rightarrow$ ♠, $\eta = 0.5 \rightarrow$ ♠, $\eta = 1 \rightarrow$ ♠

to obtain wormhole solutions. Therefore, there must have an obvious technical connection between wormhole solutions and cosmological bounce. In the Refs. [83,84] authors have discussed the existence of wormhole solutions around the cosmological bounce. So, as a final remark we can say a bounce may be occur in the Universe when WEC, NEC, SEC are not hold at some short distant interval. Hence, we can notice the bouncing conditions for F–R spacetime [31] as $\rho + 3p < 0$ and $\rho + p < 0$ corresponding to isotropic fluid as well as $\rho + p_r < 0$, $\rho + p_t < 0$ and $\rho + p_r + 2p_t < 0$ for anisotropic fluid distributions.

Since the appropriate matter distribution required to create a wormhole is still an open problem in the scientific community, so, we have considered a general anisotropic matter distribution is given by Eq. (25). Here the stress of anisotropic force can be represented by the parameter $\Delta = p_t - p_r$. Physically the nature of this stress is represented as for $\Delta < 0$ (i.e., negative), the resulting anisotropic stress is directed inward, and wormhole geometry becomes an attractive nature, whereas for $\Delta > 0$ (i.e., positive) it is directed outward and geometry becomes in repulsive nature.

3.3.1 Two models

Now, in order to verify the wormhole formation in F–R geometry, we consider two different types of matter content, which are discussed in two models apart in the following:

- **Model-1:** Let us consider the anisotropic matter distribution obeys the following relation [85]

$$p_t = \chi p_r, \tag{49}$$

where χ, anisotropic parameter may be a constant ($\neq 1$, otherwise it becomes isotropic) or a function of radial co-ordinate r. Putting the analytical expressions of p_r and p_t, derived in the respective Eqs. (40) and (41), in the above relation (49), we have derived the following explicit form of u_0' as

$$\begin{aligned} u_0' = & \frac{1}{r\left(3r\left(b'(r)+4\chi-2\right)+3(1-4\chi)b(r)+8r(\chi+1)(r-b(r))\Phi'(r)\right)} \\ & \times\Big(4e^{\Phi(r)}\Big(r\Big(2r\Big(r\Phi''(r)+\Phi'(r)\big(r\Phi'(r)-2\chi+1\big)\Big)-b'(r)\left(r\Phi'(r)+1\right)\Big)+b(r) \\ & \times\left(r\left(\Phi'(r)\left(-2r\Phi'(r)+4\chi-1\right)-2r\Phi''(r)\right)+2\chi+1\right)\Big)\Big) \end{aligned} \tag{50}$$

For simplicity, we have taken the easiest form $\chi = W_1 r^n$, where W_1 and n are some constants. Throughout the graphical representation corresponding to this model,

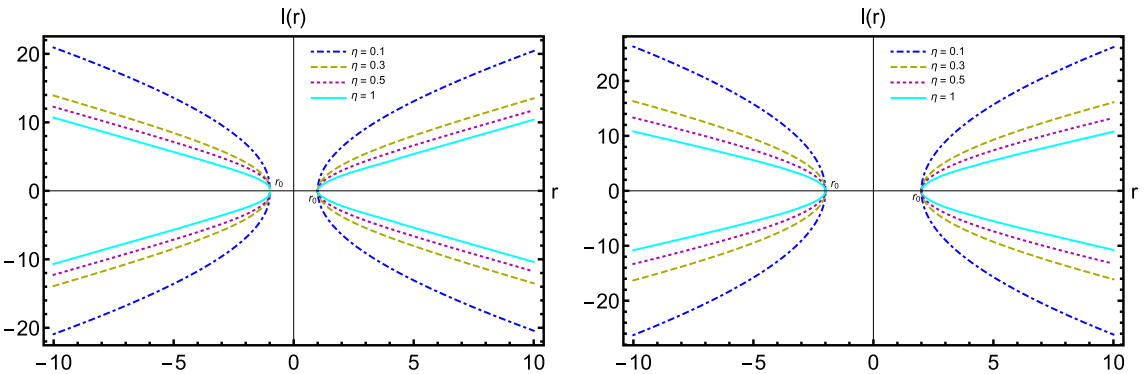

Fig. 5 Behavior of $l(r)$ against radial coordinate r corresponding to the shape function (42) for the throat radius $r_0 = 1$ (left panel) and $r_0 = 2$ (right panel)

Table 1 Some approximate numerical values of the proper radial distance $l(r)$ and the embedding surface $Z(r)$ for different variation of η corresponding to the wormhole throat $r_0 = 1kpc$

$r(kpc)$	l(r)				Z(r)			
	$\eta = 0.1$	$\eta = 0.3$	$\eta = 0.5$	$\eta = 1$	$\eta = 0.1$	$\eta = 0.3$	$\eta = 0.5$	$\eta = 1$
1.1	2.00167	1.15759	0.898159	0.637739	1.99833	1.15182	0.890705	0.627198
2	6.37739	3.74342	2.94762	2.17008	6.17298	3.56092	2.71218	1.83821
3	9.09406	5.42563	4.34015	3.31491	8.79597	4.91006	3.67643	2.38814
4	11.2303	6.80783	5.52807	4.36092	10.6828	5.86254	4.31529	2.69154
5	13.0747	8.05040	6.62982	5.37707	12.2320	6.59903	4.77628	2.87009
6	14.7381	9.21345	7.68786	6.38292	13.5609	7.19215	5.12088	2.97724
7	16.2769	10.3266	8.72185	7.38505	14.7302	7.68067	5.38309	3.04198
8	17.7242	11.4068	9.74204	8.38584	15.7763	8.08861	5.58454	3.08119
9	19.1015	12.4644	10.7541	9.38613	16.7231	8.43234	5.74018	3.10496
10	20.4235	13.5060	11.7614	10.3862	17.5876	8.72374	5.86080	3.11937

Table 2 Some approximate numerical values of the proper radial distance $l(r)$ and the embedding surface $Z(r)$ for different variation of η corresponding to the wormhole throat $r_0 = 2kpc$

$r(kpc)$	l(r)				Z(r)			
	$\eta = 0.1$	$\eta = 0.3$	$\eta = 0.5$	$\eta = 1$	$\eta = 0.1$	$\eta = 0.3$	$\eta = 0.5$	$\eta = 1$
2.1	2.86921	1.63504	1.26755	0.898159	2.82725	1.63095	1.26228	0.890705
3	8.98159	5.22876	4.08383	2.94762	8.90705	5.09968	3.91721	2.71218
4	12.7548	7.48684	5.89524	4.34015	12.544	7.12184	5.42436	3.67643
5	15.6863	9.28315	7.36823	5.52807	15.299	8.61293	6.50437	4.31529
6	18.1881	10.8513	8.68031	6.62982	17.5919	9.82012	7.35285	4.77628
7	20.4192	12.2804	9.89847	7.68786	19.5861	10.8406	8.04783	5.12088
8	22.4605	13.6157	11.0561	8.72185	21.3655	11.7251	8.63058	5.38309
9	24.3602	14.8835	12.1725	9.74208	22.9805	12.5041	9.12645	5.58454
10	26.1493	16.1008	13.2696	10.7541	24.464	13.1981	9.55255	5.74018

the constants W_1 and n are considered as -0.1 and 0.5 respectively.

- **Model-2:** In this model, we consider the matter part obeys the linear equation of state (EoS) as follows

$$p_r + \omega\rho = 0, \tag{51}$$

where ω is a positive function of radial co-ordinate r. Now for $\omega(r) < -1$ then it represents Phantom energy EoS, which have already discussed in the Ref. [68]. Utilizing the analytical expressions of ρ_r and p_r, evaluated in the respective Eqs. (39) and (40), in the above relation (51), we have derived the explicit form of u_0' as follows

$$u_0' = \frac{2e^{\Phi(r)}\left(-r\omega b'(r) + 2r(b(r) - r)\Phi'(r) + b(r)\right)}{r\left(r\omega b'(r) + 3\omega b(r) + 2r(2\omega + 1)(r - b(r))\Phi'(r) - 3b(r) - 4r\omega + 3r\right)}. \tag{52}$$

In similar way of *Model-1* for simplicity, we have also considered $\omega = W_2 r^m$ and the constants W_2 and m are taken as 3 and 2 respectively throughout the graphical representation corresponding to this model.

3.3.2 *Some specific forms of gravitational redshift function*

In order to get the energy density and pressure, we assume three cases of gravitational redshift function $\Phi(r)$.

Case-I: $\Phi(r) =$ **constant** $= K$.

Due to the choice of the redshift function $\Phi(r) =$ constant $= K$, we get the energy density and pressure in Model-1 and Model-2 in the following:

Model-1:

$$\rho(r)=\frac{e^{\eta-\frac{\eta r}{r_0}}\left(-2r_0^2(2\chi+3)\left(e^{\eta\left(\frac{r}{r_0}-1\right)}-1\right)-r_0\eta r\left(2(6\chi+1)e^{\eta\left(\frac{r}{r_0}-1\right)}-8\chi+1\right)+\eta^2r^2\right)}{24\pi r_0Gr^2\left(2r_0(2\chi-1)\left(e^{\eta\left(\frac{r}{r_0}-1\right)}-1\right)-\eta r\right)}, \tag{53}$$

$$p_r(r)=\frac{r_0\left(2e^{\eta-\frac{\eta r}{r_0}}-2\right)+\eta r\left(e^{\eta-\frac{\eta r}{r_0}}-2\right)}{8\pi Gr^2\left(\eta r-2r_0(2\chi-1)\left(e^{\eta\left(\frac{r}{r_0}-1\right)}-1\right)\right)}, \tag{54}$$

$$p_t(r)=\frac{\chi\left(r_0\left(2e^{\eta-\frac{\eta r}{r_0}}-2\right)+\eta r\left(e^{\eta-\frac{\eta r}{r_0}}-2\right)\right)}{8\pi Gr^2\left(\eta r-2r_0(2\chi-1)\left(e^{\eta\left(\frac{r}{r_0}-1\right)}-1\right)\right)}. \tag{55}$$

Model-2:

$$\rho(r)=\frac{r_0\left(-e^{\eta-\frac{\eta r}{r_0}}\right)+\eta r\left(3-2e^{\eta-\frac{\eta r}{r_0}}\right)+r_0}{8\pi Gr^2\left(r_0(4\omega-3)\left(e^{\eta\left(\frac{r}{r_0}-1\right)}-1\right)+\eta r\omega\right)}, \tag{56}$$

$$p_r(r)=\frac{\omega\left(r_0\left(e^{\eta-\frac{\eta r}{r_0}}-1\right)+\eta r\left(2e^{\eta-\frac{\eta r}{r_0}}-3\right)\right)}{8\pi Gr^2\left(r_0(4\omega-3)\left(e^{\eta\left(\frac{r}{r_0}-1\right)}-1\right)+\eta r\omega\right)}, \tag{57}$$

$$p_t(r)=\frac{e^{\eta-\frac{\eta r}{r_0}}\left(6r_0^2(\omega-1)\left(e^{\eta\left(\frac{r}{r_0}-1\right)}-1\right)+r_0\eta r\left(2(\omega-3)e^{\eta\left(\frac{r}{r_0}-1\right)}+\omega+3\right)-\eta^2r^2\omega\right)}{32\pi r_0Gr^2\left(r_0(4\omega-3)\left(e^{\eta\left(\frac{r}{r_0}-1\right)}-1\right)+\eta r\omega\right)}. \tag{58}$$

In the case-I, to verify energy conditions corresponding to our wormhole solutions we have demonstrated sufficient plots thats are included in Figs. 6 and 7 for the respective *Model-1* and *Model-2*.

- For the *Model-1*, from Fig. 6 and Table 3, we have observed that energy density (ρ) is positive for $r\in[1,\infty]$. The NEC is violated partially as $\rho+p_r\leq 0$ for all $r\in[1,\infty]$ whereas $\rho+p_t\geq 0$ for all $r\in[1,\infty]$. So, it is obvious that WEC is violated partially. Also, SEC violated as $\rho+p_r+2p_t\leq 0$ for $\eta=0.3,0.5,0.7,1$. Moreover, DEC violated partially because of $\rho-|p_r|\leq 0$ for all $r\in[1,\infty]$. So, the energy conditions like NEC, WEC, SEC, DEC are not appropriately satisfied near the wormhole throat for the *Model-1* corresponding to our solutions.
- Again for the *Model-2*, from Fig. 7 and Table 3, we have observed that ρ is positive for all $r\in[1,\infty]$ and the NEC is not satisfied partially $\rho+p_r\leq 0$ for all $r\in[1,\infty]$ whereas $\rho+p_t\geq 0$ for all $r\in[1,\infty]$. Hence WEC is violated partially in this model. The SEC is violated as $\rho+p_r+2p_t\leq 0$ for all $r\in[1.6,\infty]$ corresponding to $\eta=0.5$ and for all $r\in[1.6,\infty]$ corresponding to $\eta=0.7,1$. Also, SEC violated partially for $\eta=0.1,0.3$. The DEC is completely violated as $\rho-|p_r|\leq 0$ and $\rho-|p_t|\leq 0$ for all $r\in[1.6,\infty]$. So, as a result NEC, WEC, SEC and DEC are violated again in the *Model-2* corresponding to our solutions.

Case-II: $\Phi(r)=\log\left(\frac{\xi}{r}+1\right)$.

Due to the choice of the redshift function $\Phi(r)=\log\left(\frac{\xi}{r}+1\right)$, ($\xi$ a constant) we get the energy density and pressure in Model-1 and Model-2 in the following:

Model-1:

$$\begin{aligned}\rho(r)=&\left(e^{\eta-\frac{\eta r}{r_0}}\left(-2r_0^2\left(e^{\eta\left(\frac{r}{r_0}-1\right)}-1\right)\right.\right.\\&\times\left(\xi^2(2\chi+1)\left(16e^{\eta\left(\frac{r}{r_0}-1\right)}-9\right)+2\xi r\left((8\chi+4)e^{\eta\left(\frac{r}{r_0}-1\right)}+1\right)\right.\\&\left.+r^2(2\chi+3)\right)-r_0\eta r\left(r^2\left(2(6\chi+1)e^{\eta\left(\frac{r}{r_0}-1\right)}-8\chi+1\right)\right.\\&+\xi^2\left(2(6\chi-5)e^{\eta\left(\frac{r}{r_0}-1\right)}-8\chi+13\right)\\&\left.+2\xi r\left(4\chi\left(3e^{\eta\left(\frac{r}{r_0}-1\right)}-2\right)+3\right)\right)\\&\left.+\eta^2r^2\left(3\xi^2+r^2+4\xi r\right)\right)\Big/\\&\times\left(8\pi r_0Gr^2(\xi+r)\left(2r_0\left(e^{\eta\left(\frac{r}{r_0}-1\right)}-1\right)(\xi(2\chi-7)\right.\right.\\&\left.\left.+r(6\chi-3))-3\eta r(\xi+r)\right)\right),\end{aligned} \tag{59}$$

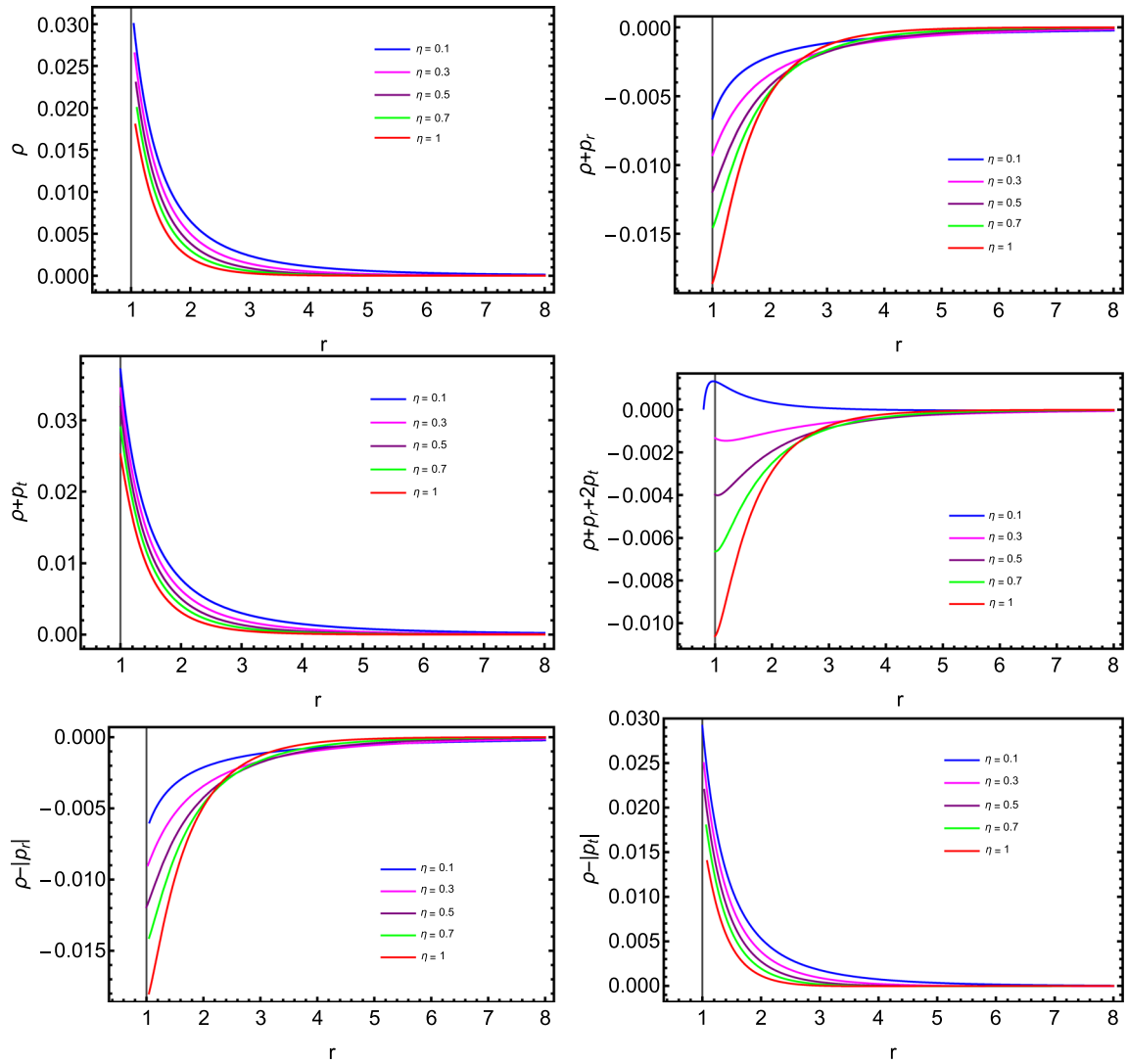

Fig. 6 Behavior of ρ, $\rho + p_r$, $\rho + p_t$, $\rho + p_r + 2p_t$, $\rho - |p_r|$ and $\rho - |p_t|$ against the radial coordinate r corresponding to $\Phi(r) = K$

$$
\begin{aligned}
p_r(r) = e^{\eta - \frac{\eta r}{r_0}} \Bigg(& \eta r \left(r^2 \left(6e^{\eta\left(\frac{r}{r_0}-1\right)} - 3 \right) \right. \\
& + 3\xi^2 \left(2e^{\eta\left(\frac{r}{r_0}-1\right)} - 1 \right) + 2\xi r \left(4e^{\eta\left(\frac{r}{r_0}-1\right)} - 1 \right) \Big) \\
& + 2r_0 \left(e^{\eta\left(\frac{r}{r_0}-1\right)} - 1 \right) \left(\xi^2 \left(16e^{\eta\left(\frac{r}{r_0}-1\right)} - 9 \right) \right. \\
& \left. + 2\xi r \left(6e^{\eta\left(\frac{r}{r_0}-1\right)} - 1 \right) + 3r^2 \right) \Bigg) \Big/ \\
& \times 8\pi G r^2 (\xi + r) \left(2r_0 \left(e^{\eta\left(\frac{r}{r_0}-1\right)} - 1 \right) (\xi(2\chi - 7) \right. \\
& \left. + r(6\chi - 3)) - 3\eta r(\xi + r) \right), \qquad (60)
\end{aligned}
$$

$$
\begin{aligned}
p_t(r) = \chi e^{\eta - \frac{\eta r}{r_0}} \Bigg(& \eta r \left(r^2 \left(6e^{\eta\left(\frac{r}{r_0}-1\right)} - 3 \right) \right. \\
& + 3\xi^2 \left(2e^{\eta\left(\frac{r}{r_0}-1\right)} - 1 \right) + 2\xi r \left(4e^{\eta\left(\frac{r}{r_0}-1\right)} - 1 \right) \Big) \\
& + 2r_0 \left(e^{\eta\left(\frac{r}{r_0}-1\right)} - 1 \right) \left(\xi^2 \left(16e^{\eta\left(\frac{r}{r_0}-1\right)} - 9 \right) \right. \\
& \left. + 2\xi r \left(6e^{\eta\left(\frac{r}{r_0}-1\right)} - 1 \right) + 3r^2 \right) \Bigg) \Big/ \\
& \times 8\pi G r^2 (\xi + r) \left(2r_0 \left(e^{\eta\left(\frac{r}{r_0}-1\right)} - 1 \right) (\xi(2\chi - 7) \right. \\
& \left. + r(6\chi - 3)) - 3\eta r(\xi + r) \right). \qquad (61)
\end{aligned}
$$

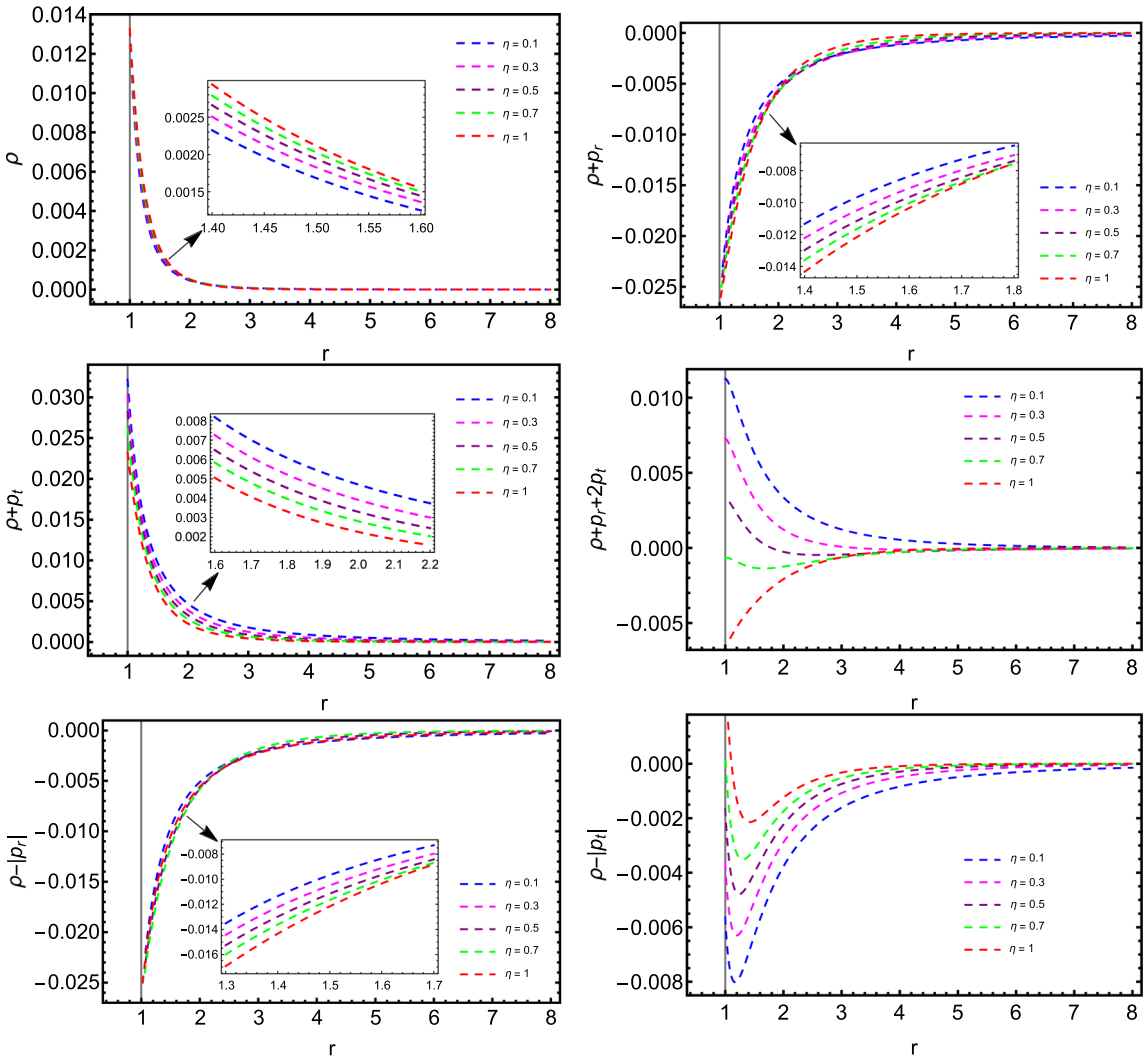

Fig. 7 Behavior of ρ, $\rho + p_r$, $\rho + p_t$, $\rho + p_r + 2p_t$, $\rho - |p_r|$ and $\rho - |p_t|$ against the radial coordinate r corresponding to $\Phi(r) = K$

Model-2:

$$\rho(r) = \frac{e^{\eta-\frac{\eta r}{r_0}}\left(r_0\left(e^{\eta\left(\frac{r}{r_0}-1\right)}-1\right)\left(\xi^2\left(16e^{\eta\left(\frac{r}{r_0}-1\right)}-9\right)+8\xi r e^{\eta\left(\frac{r}{r_0}-1\right)}+r^2\right)+\eta r(\xi+r)^2\left(3e^{\eta\left(\frac{r}{r_0}-1\right)}-2\right)\right)}{8\pi G r^2(\xi+r)\left(r_0\left(e^{\eta\left(\frac{r}{r_0}-1\right)}-1\right)(\xi(8\omega-1)+r(4\omega-3))+\eta r\omega(\xi+r)\right)}, \tag{62}$$

$$p_r(r) = -\frac{\omega e^{\eta-\frac{\eta r}{r_0}}\left(r_0\left(e^{\eta\left(\frac{r}{r_0}-1\right)}-1\right)\left(\xi^2\left(16e^{\eta\left(\frac{r}{r_0}-1\right)}-9\right)+8\xi r e^{\eta\left(\frac{r}{r_0}-1\right)}+r^2\right)+\eta r(\xi+r)^2\left(3e^{\eta\left(\frac{r}{r_0}-1\right)}-2\right)\right)}{8\pi G r^2(\xi+r)\left(r_0\left(e^{\eta\left(\frac{r}{r_0}-1\right)}-1\right)(\xi(8\omega-1)+r(4\omega-3))+\eta r\omega(\xi+r)\right)}, \tag{63}$$

Table 3 Behavior of ρ, $\rho + p_r$, $\rho + p_t$, $\rho + p_r + 2p_t$, $\rho - |p_r|$ and $\rho - |p_t|$ against the radial coordinate r, $\forall r \in [1,\infty]$ for *Model-1* and *Model-2* corresponding to $\Phi(r) = K$

Case-I: $\Phi(r) = \text{constant} = K$

Sl. no.	Terms	$\eta = 0.1$	$\eta = 0.3$	$\eta = 0.5$	$\eta = 0.7$	$\eta = 1$
Model-1						
1	ρ	$\geq 0 \ \forall r \in [1,\infty]$	$\geq 0 \ \forall r \in [1,\infty]$	$\geq 0 \ \forall r \in [1,\infty]$	$\geq 0 \ \forall r \in [1,\infty]$	$\geq 0 \ \forall r \in [1,\infty]$
2	$\rho + p_r$	$\leq 0 \ \forall r \in [1,\infty]$	$\leq 0 \ \forall r \in [1,\infty]$	$\leq 0 \ \forall r \in [1,\infty]$	$\leq 0 \ \forall r \in [1,\infty]$	$\leq 0 \ \forall r \in [1,\infty]$
3	$\rho + p_t$	$\geq 0 \ \forall r \in [1,\infty]$	$\geq 0 \ \forall r \in [1,\infty]$	$\geq 0 \ \forall r \in [1,\infty]$	$\geq 0 \ \forall r \in [1,\infty]$	$\geq 0 \ \forall r \in [1,\infty]$
4	$\rho + p_r + 2p_t$	$\geq 0 \ \forall r \in [1,\infty]$	$\leq 0 \ \forall r \in [1,\infty]$	$\leq 0 \ \forall r \in [1,\infty]$	$\leq 0 \ \forall r \in [1,\infty]$	$\leq 0 \ \forall r \in [1,\infty]$
5	$\rho - \lvert p_r \rvert$	$\leq 0 \ \forall r \in [1,\infty]$	$\leq 0 \ \forall r \in [1,\infty]$	$\leq 0 \ \forall r \in [1,\infty]$	$\leq 0 \ \forall r \in [1,\infty]$	$\leq 0 \ \forall r \in [1,\infty]$
6	$\rho - \lvert p_t \rvert$	$\geq 0 \ \forall r \in [1,\infty]$	$\geq 0 \ \forall r \in [1,\infty]$	$\geq 0 \ \forall r \in [1,\infty]$	$\geq 0 \ \forall r \in [1,\infty]$	$\geq 0 \ \forall r \in [1,\infty]$
Model-2						
1	ρ	$\geq 0 \ \forall r \in [1,\infty]$	$\geq 0 \ \forall r \in [1,\infty]$	$\geq 0 \ \forall r \in [1,\infty]$	$\geq 0 \ \forall r \in [1,\infty]$	$\geq 0 \ \forall r \in [1,\infty]$
2	$\rho + p_r$	$\leq 0 \ \forall r \in [1,\infty]$	$\leq 0 \ \forall r \in [1,\infty]$	$\leq 0 \ \forall r \in [1,\infty]$	$\leq 0 \ \forall r \in [1,\infty]$	$\leq 0 \ \forall r \in [1,\infty]$
3	$\rho + p_t$	$\geq 0 \ \forall r \in [1,\infty]$	$\geq 0 \ \forall r \in [1,\infty]$	$\geq 0 \ \forall r \in [1,\infty]$	$\geq 0 \ \forall r \in [1,\infty]$	$\geq 0 \ \forall r \in [1,\infty]$
4	$\rho + p_r + 2p_t$	$\geq 0 \ \forall r \in [1,\infty]$	$\geq 0 \ \forall r \in [1,\infty]$	$\geq 0 \ \forall r \in [1,1.6) \leq 0 \ \forall r \in [1.6,\infty]$	$\leq 0 \ \forall r \in [1,\infty]$	$\leq 0 \ \forall r \in [1,\infty]$
5	$\rho - \lvert p_r \rvert$	$\leq 0 \ \forall r \in [1,\infty]$	$\leq 0 \ \forall r \in [1,\infty]$	$\leq 0 \ \forall r \in [1,\infty]$	$\leq 0 \ \forall r \in [1,\infty]$	$\leq 0 \ \forall r \in [1,\infty]$
6	$\rho - \lvert p_t \rvert$	$\leq 0 \ \forall r \in [1,\infty]$	$\leq 0 \ \forall r \in [1,\infty]$	$\leq 0 \ \forall r \in [1,\infty]$	$\leq 0 \ \forall r \in [1,\infty]$	$\leq 0 \ \forall r \in [1.15,\infty]$

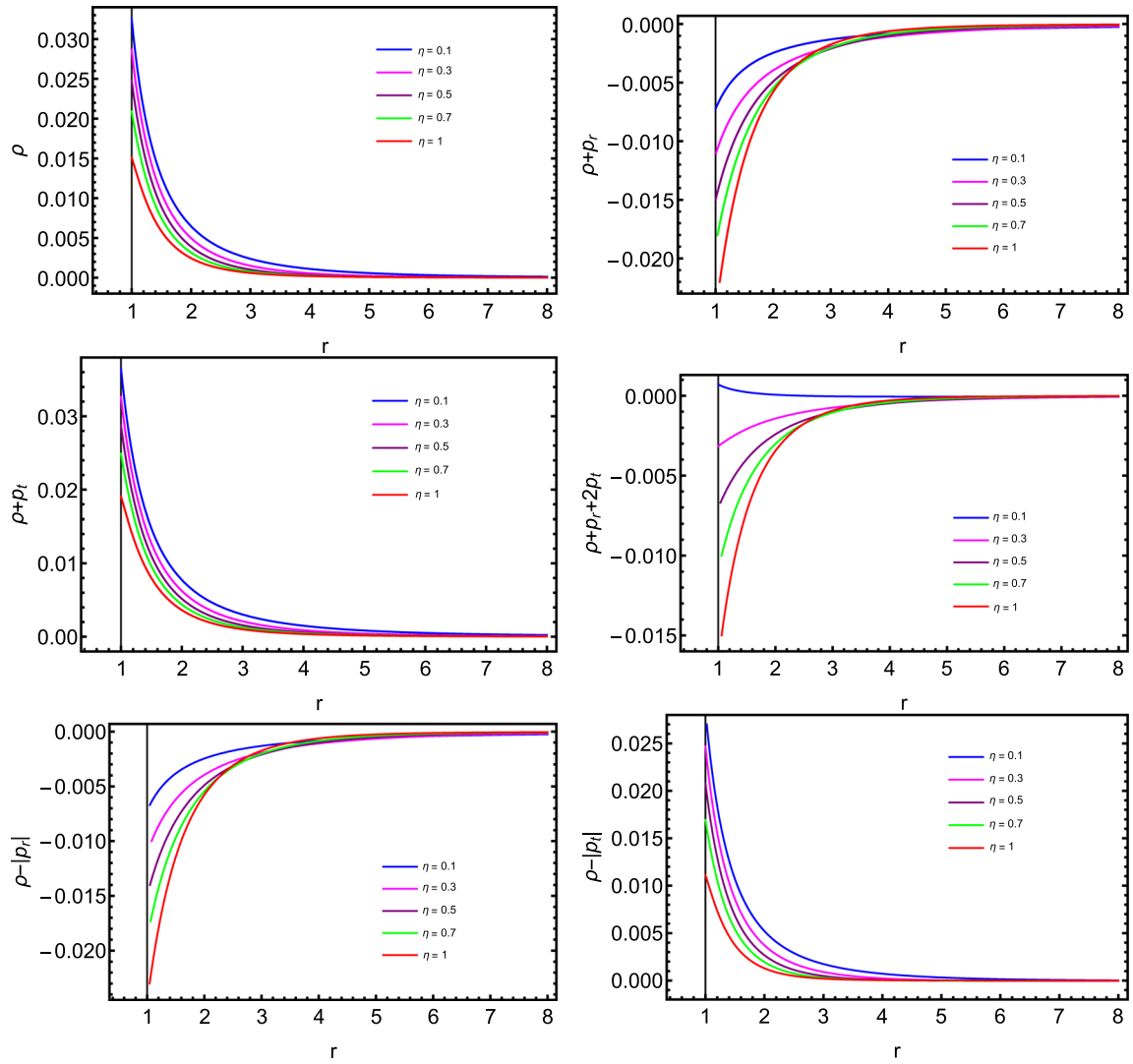

Fig. 8 Behavior of ρ, $\rho + p_r$, $\rho + p_t$, $\rho + p_r + 2p_t$, $\rho - |p_r|$ and $\rho - |p_t|$ against the radial coordinate r corresponding to $\Phi(r) = \log\left(\frac{\xi}{r} + 1\right)$

$$
\begin{aligned}
p_t(r) = &\left(e^{\eta-\frac{\eta r}{r_0}}\left(2r_0^2\left(e^{\eta\left(\frac{r}{r_0}-1\right)}-1\right)\right.\right.\\
&\times\left(\xi^2(\omega-1)\left(16e^{\eta\left(\frac{r}{r_0}-1\right)}-9\right)\right.\\
&+2\xi r\left((4\omega-6)e^{\eta\left(\frac{r}{r_0}-1\right)}+\omega+1\right)\\
&\left.+3r^2(\omega-1)\right)+r_0\eta r\left(r^2\left(2(\omega-3)e^{\eta\left(\frac{r}{r_0}-1\right)}+\omega+3\right)\right.\\
&-\xi^2\left(2(5\omega+3)e^{\eta\left(\frac{r}{r_0}-1\right)}-13\omega-3\right)\\
&\left.\left.-2\xi r\left(4e^{\eta\left(\frac{r}{r_0}-1\right)}-3\omega-1\right)\right)\right.\\
&\left.-\eta^2r^2\omega\left(3\xi^2+r^2+4\xi r\right)\right)\Big)\Big/\left(32\pi r_0Gr^2(\xi+r)\right.\\
&\times\left(r_0\left(e^{\eta\left(\frac{r}{r_0}-1\right)}-1\right)(\xi(8\omega-1)\right.\\
&\left.\left.+r(4\omega-3))+\eta r\omega(\xi+r)\right)\right).
\end{aligned}
\tag{64}
$$

In this case, we have scrutinized all required energy conditions by illustrating several plots in Figs. 8 and 9 corresponding to the *Model-1* and *Model-2* respectively.

- From Fig. 8 and Table 4 corresponding to the *Model-1*, we have noticed that energy density (ρ) is positive for $r \in [1, \infty]$. The NEC is partially violated because of $\rho + p_r \leq 0$ for all $r \in [1, \infty]$. Although $\rho + p_t \geq 0$ for all $r \in [1, \infty]$ however, the SEC is violated as $\rho + p_r + 2p_t \leq 0$ for all $r \in [1, \infty]$ corresponding to $\eta = 0.3, 0.5, 0.7, 1$ except $\eta = 0.1$. So, SEC is not satisfied

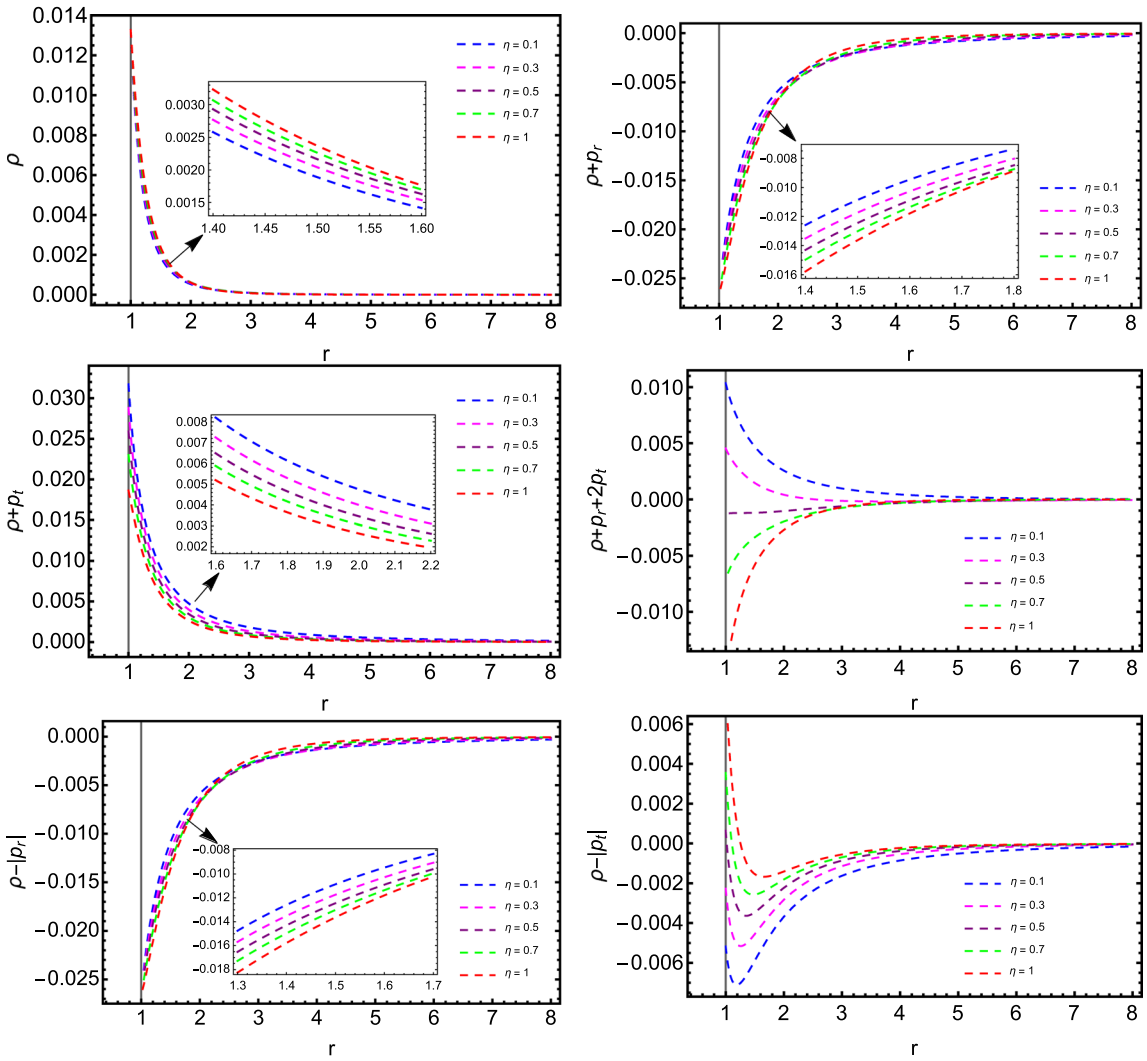

Fig. 9 Behavior of ρ, $\rho + p_r$, $\rho + p_t$, $\rho + p_r + 2p_t$, $\rho - |p_r|$ and $\rho - |p_t|$ against the radial coordinate r corresponding to $\Phi(r) = \log\left(\frac{\xi}{r} + 1\right)$

in this model. As NEC is violated partially, the WEC obviously partially violated. Moreover, DEC is violated partially as $\rho - |p_r| \leq 0$ for all $r \in [1, \infty]$. Therefore, NEC, WEC, SEC and DEC are not satisfied properly in the *Model-1* corresponding to our wormhole solutions.

- Again From Fig. 9 and Table 4 for the *Model-2*, we have noticed that $\rho \geq 0$ for all $r \in [1, \infty]$. Next the NEC is partially violated as $\rho + p_r \leq 0$ for all $r \in [1, \infty]$ and hence WEC is also partially satisfied as WEC $\subset$ NEC. Further $\rho + p_r 2p_t \leq 0$ for all $r \in [1, \infty]$ corresponding to $\eta = 0.5, 0.7, 1$ but $\rho + p_r 2p_t \geq 0$ for all $r \in [1, \infty]$ for $\eta = 0.1, 0.3$. So, we can say the SEC violated partially in this model. Again, DEC is violated completely as $\rho - |p_r \leq 0|$ for all $r \in [1, \infty]$ and $\rho - |p_t \leq 0|$ for the ranges of r, given in the Table 4 with details. So, as a result, we have NEC, WEC, SEC and DEC are not satisfied properly corresponding to our wormhole solutions in this model.

Case-III: $\Phi(r) = e^{-\gamma/r}$.

Due to the choice of the redshift function $\Phi(r) = e^{-\gamma/r}$, (γ a constant) we get the energy density and pressure in Model-1 and Model-2 in the following:

Model-1:

$$\rho(r) = \left(e^{-\frac{\eta r}{r_0}+\eta-\frac{2\gamma}{r}}\left(\eta^2 r^4 e^{\frac{2\gamma}{r}}\left(re^{\gamma/r} - 2\gamma\right)\right.\right.$$
$$-r_0\eta r^2 e^{\gamma/r}\left(2r^2(6\chi+1)e^{\frac{\eta r}{r_0}-\eta+\frac{2\gamma}{r}} - 4\gamma^2 e^{\eta\left(\frac{r}{r_0}-1\right)}\right.$$
$$+4\gamma(\gamma+r)e^{\frac{\eta r}{r_0}-\eta+\frac{\gamma}{r}} + 4\gamma^2 - r^2(8\chi-1)e^{\frac{2\gamma}{r}}$$
$$\left.-4\gamma e^{\gamma/r}(\gamma+r)\right) - 2r_0^2\left(e^{\eta\left(\frac{r}{r_0}-1\right)} - 1\right)$$
$$\times\left(-8\gamma^3 e^{\eta\left(\frac{r}{r_0}-1\right)} - 8\gamma^2(\gamma - 2r(\chi+1))e^{\frac{\eta r}{r_0}-\eta+\frac{\gamma}{r}}\right.$$
$$-8\gamma r(-\gamma+2r\chi+r)e^{\frac{\eta r}{r_0}-\eta+\frac{2\gamma}{r}} + 8\gamma^3$$
$$+r^3(2\chi+3)e^{\frac{3\gamma}{r}} + 8\gamma^2 e^{\gamma/r}$$

$$\times(\gamma-2r(\chi+1))+4\gamma re^{\frac{2\gamma}{r}}(-2\gamma+r\chi+r)\Big)\Big)\Big)\Big/$$
$$\times\Big(8\pi r_0Gr^4\Big(2r_0\left(e^{\eta\left(\frac{r}{r_0}-1\right)}-1\right)$$
$$\times\left(4\gamma(\chi+1)+3r(2\chi-1)e^{\gamma/r}\right)-3\eta r^2e^{\gamma/r}\Big)\Big) \tag{65}$$

$$p_r(r)=\Big(e^{-\frac{\eta r}{r_0}-\eta-\frac{2\gamma}{r}}\Big(2r_0\Big(-3r^3e^{\frac{\eta r}{r_0}+\eta+\frac{3\gamma}{r}}$$
$$+8\gamma^3e^{\frac{\eta r}{r_0}+\eta}-4\gamma^3e^{\frac{2\eta r}{r_0}}+4\gamma^2(2\gamma+5r)e^{\frac{\eta r}{r_0}+\eta+\frac{\gamma}{r}}$$
$$-2\gamma^2(2\gamma+5r)e^{\frac{2\eta r}{r_0}+\frac{\gamma}{r}}+6\gamma r(2r-\gamma)e^{\frac{2\eta r}{r_0}+\frac{2\gamma}{r}}$$
$$-4\gamma r(5r-3\gamma)e^{\frac{\eta r}{r_0}+\eta+\frac{2\gamma}{r}}-4\gamma^3e^{2\eta}+3r^3e^{2\eta+\frac{3\gamma}{r}}$$
$$-2\gamma^2(2\gamma+5r)e^{2\eta+\frac{\gamma}{r}}+2\gamma r(4r-3\gamma)$$
$$\times e^{2(\eta+\frac{\gamma}{r})}\Big)+\eta r^2e^{\eta+\frac{\gamma}{r}}\Big(-6r^2e^{\frac{\eta r}{r_0}+\frac{2\gamma}{r}}-4\gamma^2e^{\frac{\eta r}{r_0}}$$
$$-4\gamma re^{\frac{\eta r}{r_0}+\frac{\gamma}{r}}+4\gamma^2e^{\eta}+3r^2e^{\eta+\frac{2\gamma}{r}}+4\gamma re^{\eta+\frac{\gamma}{r}}\Big)\Big)\Big)\Big/$$
$$\times\Big(8\pi Gr^4\Big(3\eta r^2e^{\gamma/r}-2r_0\left(e^{\eta\left(\frac{r}{r_0}-1\right)}-1\right)$$
$$\times\left(4\gamma(\chi+1)+3r(2\chi-1)e^{\gamma/r}\right)\Big) \tag{66}$$

$$p_t(r)=\Big(\chi e^{-\frac{\eta r}{r_0}-\eta-\frac{2\gamma}{r}}\Big(2r_0\Big(-3r^3e^{\frac{\eta r}{r_0}+\eta+\frac{3\gamma}{r}}$$
$$+8\gamma^3e^{\frac{\eta r}{r_0}+\eta}-4\gamma^3e^{\frac{2\eta r}{r_0}}+4\gamma^2(2\gamma+5r)e^{\frac{\eta r}{r_0}+\eta+\frac{\gamma}{r}}$$
$$-2\gamma^2(2\gamma+5r)e^{\frac{2\eta r}{r_0}+\frac{\gamma}{r}}$$
$$+6\gamma r(2r-\gamma)e^{\frac{2\eta r}{r_0}+\frac{2\gamma}{r}}-4\gamma r(5r-3\gamma)e^{\frac{\eta r}{r_0}+\eta+\frac{2\gamma}{r}}$$
$$-4\gamma^3e^{2\eta}+3r^3e^{2\eta+\frac{3\gamma}{r}}-2\gamma^2(2\gamma+5r)e^{2\eta+\frac{\gamma}{r}}$$
$$+2\gamma r(4r-3\gamma)e^{2(\eta+\frac{\gamma}{r})}\Big)+\eta r^2e^{\eta+\frac{\gamma}{r}}\Big(-6r^2e^{\frac{\eta r}{r_0}+\frac{2\gamma}{r}}$$
$$-4\gamma^2e^{\frac{\eta r}{r_0}}-4\gamma re^{\frac{\eta r}{r_0}+\frac{\gamma}{r}}+4\gamma^2e^{\eta}+3r^2e^{\eta+\frac{2\gamma}{r}}$$
$$+4\gamma re^{\eta+\frac{\gamma}{r}}\Big)\Big)\Big)\Big/\Big(8\pi Gr^4\left(3\eta r^2e^{\gamma/r}-2r_0\left(e^{\eta\left(\frac{r}{r_0}-1\right)}-1\right)\right.$$
$$\times\left.\left(4\gamma(\chi+1)+3r(2\chi-1)e^{\gamma/r}\right)\right) \tag{67}$$

Model-2:

$$\rho(r)=e^{-\frac{\eta r}{r_0}+\eta-\frac{\gamma}{r}}\Big(r_0\left(e^{\eta\left(\frac{r}{r_0}-1\right)}-1\right)$$
$$\times\Big(8\gamma^2e^{\eta\left(\frac{r}{r_0}-1\right)}-8\gamma re^{\frac{\eta r}{r_0}-\eta+\frac{\gamma}{r}}-8\gamma^2+r^2e^{\frac{2\gamma}{r}}+2\gamma re^{\gamma/r}\Big)\eta r^3$$
$$+e^{\frac{2\gamma}{r}}\left(3e^{\eta\left(\frac{r}{r_0}-1\right)}-2\right)\Big)\Big/8\pi Gr^3\Big(r_0\left(e^{\eta\left(\frac{r}{r_0}-1\right)}-1\right)$$
$$\left(r(4\omega-3)e^{\gamma/r}-2(2\gamma\omega+\gamma)\right)+\eta r^2\omega e^{\gamma/r}\Big) \tag{68}$$

$$p_r(r)=-e^{-\frac{\eta r}{r_0}+\eta-\frac{\gamma}{r}}\omega\Big(\eta r^3e^{\frac{2\gamma}{r}}\left(3e^{\eta\left(\frac{r}{r_0}-1\right)}-2\right)$$
$$+r_0\left(e^{\eta\left(\frac{r}{r_0}-1\right)}-1\right)\Big(8\gamma^2e^{\eta\left(\frac{r}{r_0}-1\right)}$$
$$-8\gamma re^{\frac{\eta r}{r_0}-\eta+\frac{\gamma}{r}}-8\gamma^2+r^2e^{\frac{2\gamma}{r}}+2\gamma re^{\gamma/r}\Big)\Big)\Big/8\pi$$
$$\times Gr^3\Big(r_0\left(e^{\eta\left(\frac{r}{r_0}-1\right)}-1\right)\left(r(4\omega-3)e^{\gamma/r}-2(2\gamma\omega+\gamma)\right)$$
$$+\eta r^2\omega e^{\gamma/r}\Big) \tag{69}$$

$$p_t(r)=\frac{e^{-\frac{2\gamma}{r}}\left(1-e^{\eta-\frac{\eta r}{r_0}}\right)}{32\pi Gr^4}\times\Bigg(\frac{2\left(\gamma+re^{\gamma/r}\right)\left(2r_0\gamma\left(e^{\eta\left(\frac{r}{r_0}-1\right)}-1\right)+\eta r^2e^{\gamma/r}\right)}{r_0\left(e^{\eta\left(\frac{r}{r_0}-1\right)}-1\right)}+4\gamma e^{\gamma/r}(\gamma-2r)$$
$$+\frac{re^{\gamma/r}\left(2r_0\left(3re^{\gamma/r}-4\gamma\right)\left(e^{\eta\left(\frac{r}{r_0}-1\right)}-1\right)+3\eta r^2e^{\gamma/r}\right)\left(r_0\left(2\gamma e^{\eta\left(\frac{r}{r_0}-1\right)}-2\gamma+r(\omega-1)e^{\gamma/r}\right)-\eta r^2\omega e^{\gamma/r}\right)}{r_0\left(e^{\eta\left(\frac{r}{r_0}-1\right)}-1\right)\left(r_0\left(e^{\eta\left(\frac{r}{r_0}-1\right)}-1\right)\left(r(4\omega-3)e^{\gamma/r}-2(2\gamma\omega+\gamma)\right)+\eta r^2\omega e^{\gamma/r}\right)}\Bigg) \tag{70}$$

In this case, for the better understanding of energy conditions, we have drawn several plots, which are depicted in Figs. 10 and 11 corresponding to the *Model-1* and *Model-2* respectively.

- For the *Model-1*, after scrutinized Fig. 10 and Table 5, we have energy density (ρ) is positive for all $r\in[1,\infty]$. The NEC is partially violated because of $\rho+p_r\leq 0$ for $r\in[1,\infty]$ and hence WEC is also violated partially for each selected values $\eta=0.1,0.3,0.5,0.7,1$. Further the SEC is not satisfied as $\rho+p_r+2p_t\leq 0$ for all $r\in[1,\infty]$ corresponding to $\eta=0.3,0.5,0.7,1$ but for $\eta=0.1$ $\rho+p_r+2p_t\geq 0$ and $\rho+p_r\leq 0$ for each of $\eta=0.1,0.3,0.5,0.7,1$ with $r\in[1,\infty]$. Also, the DEC is partially violated as $\rho-|p_r|\leq 0$ for all $r\in[1,\infty]$. Thus in this model, energy conditions are not properly hold near the throat corresponding to our proposed wormhole solutions.
- After examined Fig. 11 and Table 5, we have noticed that $\rho\geq 0$ for all $r\in[1,\infty]$. Next $\rho+p_r\leq 0$

Table 4 Behavior of ρ, $\rho + p_r$, $\rho + p_t$, $\rho + p_r + 2p_t$, $\rho - |p_r|$ and $\rho - |p_t|$ against the radial coordinate r, $\forall r \in [1,\infty]$ for *Model-1* and *Model-2* corresponding to $\Phi(r) = \log\left(\frac{\xi}{r} + 1\right)$

Case-II: $\Phi(r) = \log\left(\frac{\xi}{r} + 1\right)$						
Sl. no.	Terms	$\eta = 0.1$	$\eta = 0.3$	$\eta = 0.5$	$\eta = 0.7$	$\eta = 1$
Model-1						
1	ρ	$\geq 0 \ \forall r \in [1,\infty]$	$\geq 0 \ \forall r \in [1,\infty]$	$\geq 0 \ \forall r \in [1,\infty]$	$\geq 0 \ \forall r \in [1,\infty]$	$\geq 0 \ \forall r \in [1,\infty]$
2	$\rho + p_r$	$\leq 0 \ \forall r \in [1,\infty]$	$\leq 0 \ \forall r \in [1,\infty]$	$\leq 0 \ \forall r \in [1,\infty]$	$\leq 0 \ \forall r \in [1,\infty]$	$\leq 0 \ \forall r \in [1,\infty]$
3	$\rho + p_t$	$\geq 0 \ \forall r \in [1,\infty]$	$\geq 0 \ \forall r \in [1,\infty]$	$\geq 0 \ \forall r \in [1,\infty]$	$\geq 0 \ \forall r \in [1,\infty]$	$\geq 0 \ \forall r \in [1,\infty]$
4	$\rho + p_r + 2p_t$	$\geq 0 \ \forall r \in [1,\infty]$	$\leq 0 \ \forall r \in [1,\infty]$	$\leq 0 \ \forall r \in [1,\infty]$	$\leq 0 \ \forall r \in [1,\infty]$	$\leq 0 \ \forall r \in [1,\infty]$
5	$\rho - \lvert p_r \rvert$	$\leq 0 \ \forall r \in [1,\infty]$	$\leq 0 \ \forall r \in [1,\infty]$	$\leq 0 \ \forall r \in [1,\infty]$	$\leq 0 \ \forall r \in [1,\infty]$	$\leq 0 \ \forall r \in [1,\infty]$
6	$\rho - \lvert p_t \rvert$	$\geq 0 \ \forall r \in [1,\infty]$	$\geq 0 \ \forall r \in [1,\infty]$	$\geq 0 \ \forall r \in [1,\infty]$	$\geq 0 \ \forall r \in [1,\infty]$	$\geq 0 \ \forall r \in [1,\infty]$
Model-2						
1	ρ	$\geq 0 \ \forall r \in [1,\infty]$	$\geq 0 \ \forall r \in [1,\infty]$	$\geq 0 \ \forall r \in [1,\infty]$	$\geq 0 \ \forall r \in [1,\infty]$	$\geq 0 \ \forall r \in [1,\infty]$
2	$\rho + p_r$	$\leq 0 \ \forall r \in [1,\infty]$	$\leq 0 \ \forall r \in [1,\infty]$	$\leq 0 \ \forall r \in [1,\infty]$	$\leq 0 \ \forall r \in [1,\infty]$	$\leq 0 \ \forall r \in [1,\infty]$
3	$\rho + p_t$	$\geq 0 \ \forall r \in [1,\infty]$	$\geq 0 \ \forall r \in [1,\infty]$	$\geq 0 \ \forall r \in [1,\infty]$	$\geq 0 \ \forall r \in [1,\infty]$	$\geq 0 \ \forall r \in [1,\infty]$
4	$\rho + p_r + 2p_t$	$\geq 0 \ \forall r \in [1,\infty]$	$\geq 0 \ \forall r \in [1,\infty]$	$\leq 0 \ \forall r \in [1,\infty]$	$\leq 0 \ \forall r \in [1,\infty]$	$\leq 0 \ \forall r \in [1,\infty]$
5	$\rho - \lvert p_r \rvert$	$\leq 0 \ \forall r \in [1,\infty]$	$\leq 0 \ \forall r \in [1,\infty]$	$\leq 0 \ \forall r \in [1,\infty]$	$\leq 0 \ \forall r \in [1,\infty]$	$\leq 0 \ \forall r \in [1,\infty]$
6	$\rho - \lvert p_t \rvert$	$\leq 0 \ \forall r \in [1,\infty]$	$\leq 0 \ \forall r \in [1,\infty]$	$\leq 0 \ \forall r \in [1,\infty]$	$\geq 0 \ \forall r \in [1,1.1) \leq 0 \ \forall r \in [1.1,\infty]$	$\geq 0 \ \forall r \in [1,1.2) \leq 0 \ \forall r \in [1.2,\infty]$

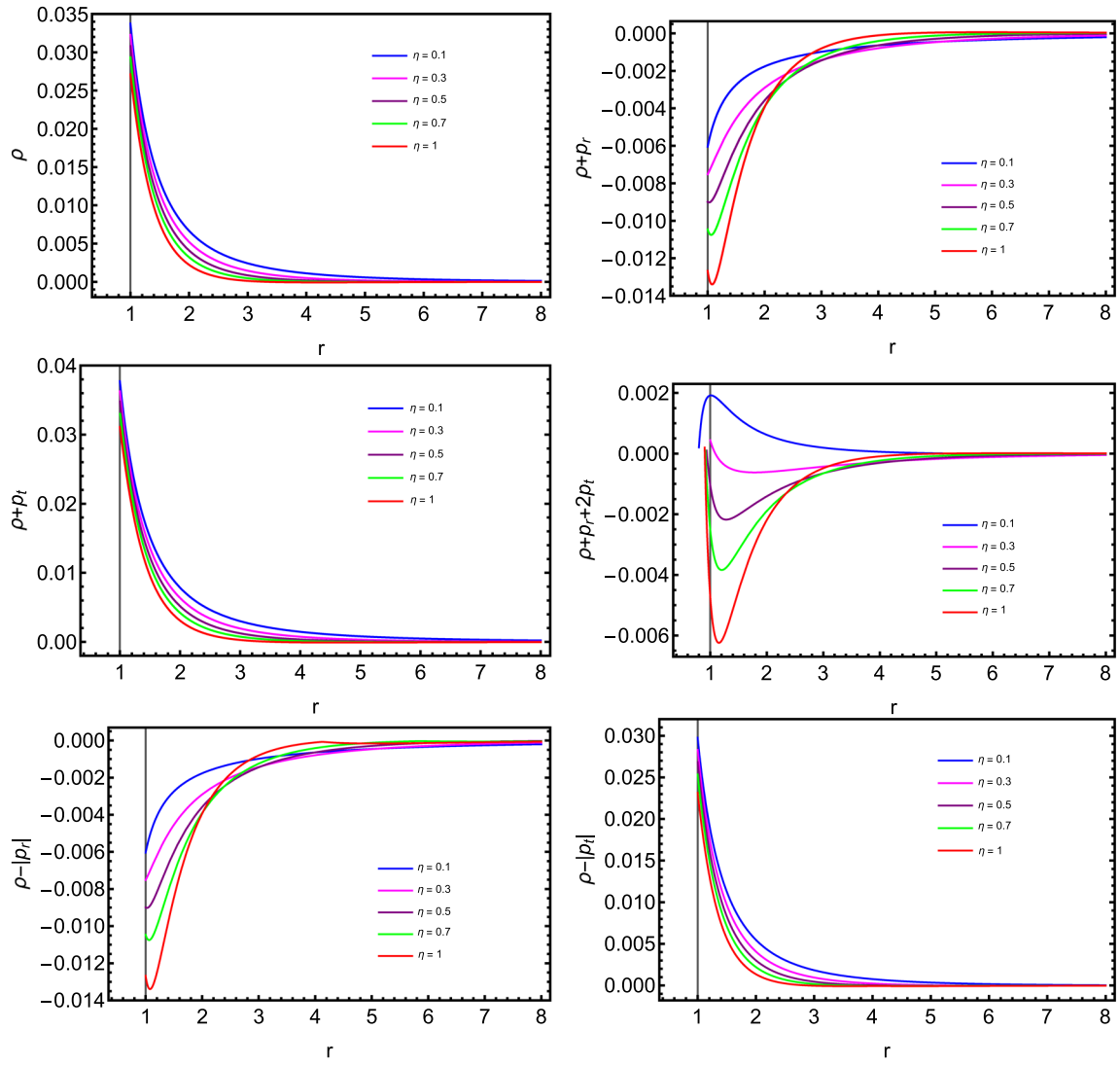

Fig. 10 Behavior of ρ, $\rho + p_r$, $\rho + p_t$, $\rho + p_r + 2p_t$, $\rho - |p_r|$ and $\rho - |p_t|$ against the radial coordinate r corresponding to $\Phi(r) = e^{-\gamma/r}$

for all $r \in [1, \infty]$ and corresponding to each of $\eta = 0.1, 0.3, 0.5, 0.7, 1$ and hence the NEC as well as WEC is violated partially. Further $\rho + p_r + 2p_t \geq 0$ for all $r \in [1, \infty]$ with $\eta = 0.1, 0.3$ but for $\eta = 0.5, 0.7, 1$, $\rho + p_r + 2p_t \geq 0$ and as well $\leq$ corresponding to the range of r have reported in details in the Table 5. So, we can say the SEC is not satisfied in this model. Again, the DEC is completely violated as both of $\rho - |p_r|$ and $\rho - |p_t|$ are ≤ 0 for all $r \in [1, \infty]$ and each of $\eta = 0.1, 0.3, 0.5, 0.7, 1$. Therefore, in the *Model-2* the all of NEC, WEC, SEC, DEC are not hold appropriately near the throat of our proposed wormhole solutions.

4 Average null energy condition (ANEC) violating matter

In this section, we will discuss the "volume integral quantifier", which basically provides the information about the total amount of exotic matter required to maintains the wormhole structure. According to Visser et al., this quantity only related to ρ and p_r but not to tangential pressure p_t and is defined in the following integral form [76]

$$\mathcal{I}_v = \oint [\rho + p_r]\, dV = 2 \int_{r_0}^{\infty} 4\pi r^2 (\rho + p_r)\, dr, \tag{71}$$

where $dV = r^2 \sin\theta dr d\theta d\phi$. By imposing a cutoff of the energy–momentum tensor at $R \geq r_0$, we can rewritten the

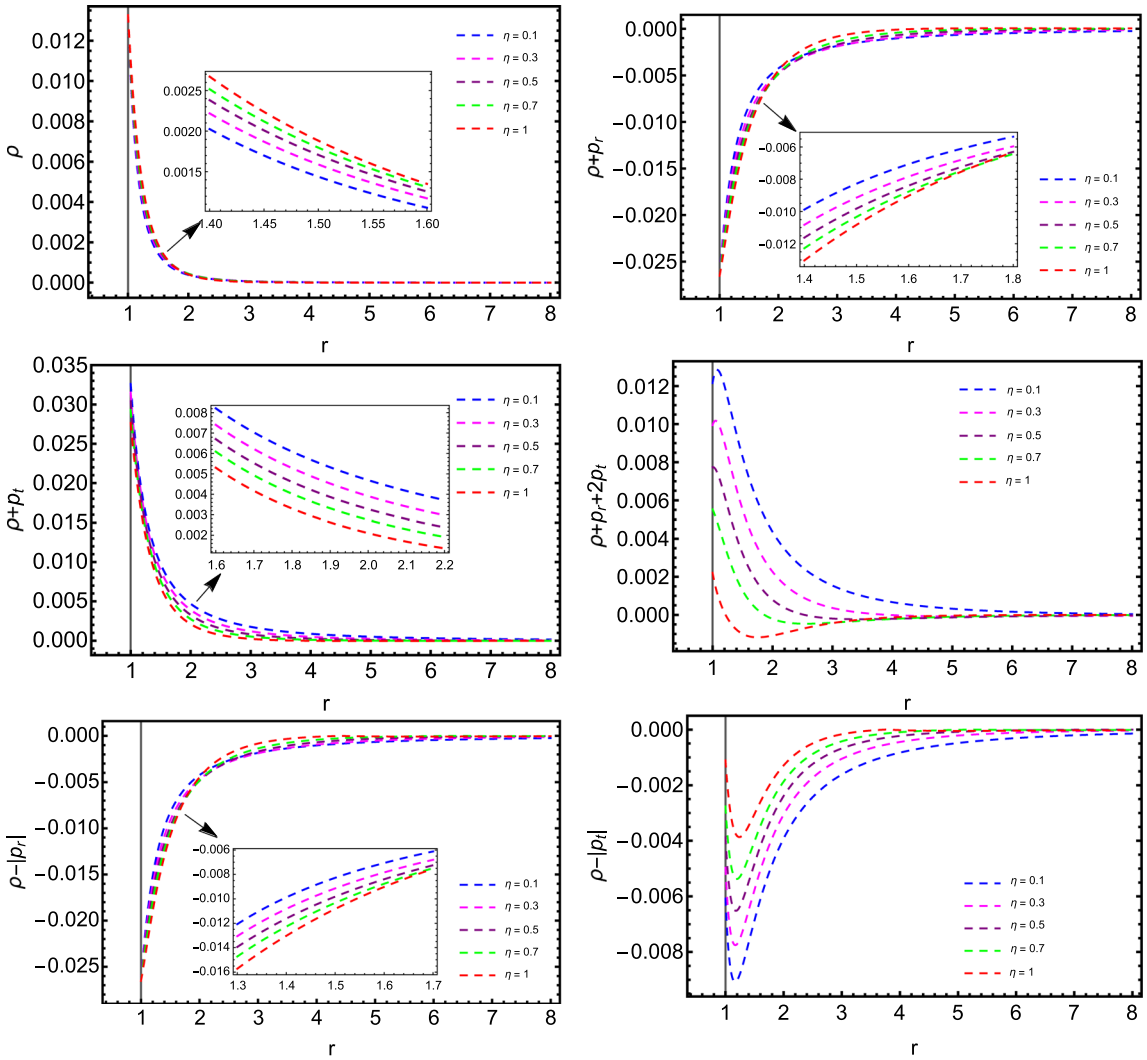

Fig. 11 Behavior of ρ, $\rho + p_r$, $\rho + p_t$, $\rho + p_r + 2p_t$, $\rho - |p_r|$ and $\rho - |p_t|$ against the radial coordinate r corresponding to $\Phi(r) = e^{-\gamma/r}$

integral (71) as

$$\mathcal{I}_v = 8\pi \int_{r_0}^{R} (\rho + p_r)\, r^2 dr, \tag{72}$$

where r_0 is the throat radius. Now, putting the expression of $\rho + p_r$ in the above Eq. (72), one can straightforwardly evaluate the integral $\mathcal{I}_v$. Here an important fact that when $R \to r_0$ the integral $\mathcal{I}_v$ must be $\to 0$. Due to the complicated explicit expression of $\mathcal{I}_v$, we examined the nature of the integral against r graphically, included in Figs. 12, 13 and 14. From these figures, we have observed that ANEC is violated near the wormhole throat for *Mode-1* and *Model-2* in each of cases—I, II, III. So, this nature of $\mathcal{I}_v$ confirms the existence of exotic matter near the wormhole throat, and we can minimize the total amount of exotic matter by changing the values of our model parameters. Therefore, our proposed spacetime geometries may be demonstrated the existence of traversable wormhole geometry.

5 Discussions and conclusions

In the present article, we have explored our goal in two parts: firstly, gravitational field equations in Finsler–Randers geometry are constructed for a static, spherically symmetric line element, and secondly, the formation of traversable wormhole has been examined in this geometry. To the best of our knowledge, this is the first attempt at the construction of gravitational field equations in F–R geometry corresponding to spherically symmetric metric and examining traversable wormhole configuration in this geometry. For this purpose, we have deduced the modified field equations corresponding to Morris–Thorne wormhole geometry. Next, we have selected the shape function as in the form $b(r) = \frac{r}{exp\left(\eta\left(\frac{r}{r_0}-1\right)\right)}$ with arbitrary constant parameter η and radius of wormhole throat r_0. For a better visualization of wormhole shape, we have included two-dimensional and

Table 5 Behavior of ρ, $\rho + p_r$, $\rho + p_t$, $\rho + p_r + 2p_t$, $\rho - |p_r|$ and $\rho - |p_t|$ against the radial coordinate r, $\forall r \in [1,\infty]$ for *Model-1* and *Model-2* corresponding to $\Phi(r) = e^{-\gamma/r}$

Case-III: $\Phi(r) = e^{-\gamma/r}$						
Sl. no.	Terms	$\eta = 0.1$	$\eta = 0.3$	$\eta = 0.5$	$\eta = 0.7$	$\eta = 1$
Model-1						
1	ρ	$\geq 0 \ \forall r \in [1,\infty]$	$\geq 0 \ \forall r \in [1,\infty]$	$\geq 0 \ \forall r \in [1,\infty]$	$\geq 0 \ \forall r \in [1,\infty]$	$\geq 0 \ \forall r \in [1,\infty]$
2	$\rho + p_r$	$\leq 0 \ \forall r \in [1,\infty]$	$\leq 0 \ \forall r \in [1,\infty]$	$\leq 0 \ \forall r \in [1,\infty]$	$\leq 0 \ \forall r \in [1,\infty]$	$\leq 0 \ \forall r \in [1,\infty]$
3	$\rho + p_t$	$\geq 0 \ \forall r \in [1,\infty]$	$\geq 0 \ \forall r \in [1,\infty]$	$\geq 0 \ \forall r \in [1,\infty]$	$\geq 0 \ \forall r \in [1,\infty]$	$\geq 0 \ \forall r \in [1,\infty]$
4	$\rho + p_r + 2p_t$	$\geq 0 \ \forall r \in [1,\infty]$	$\leq 0 \ \forall r \in [1,\infty]$	$\leq 0 \ \forall r \in [1,\infty]$	$\leq 0 \ \forall r \in [1,\infty]$	$\leq 0 \ \forall r \in [1,\infty]$
5	$\rho - \lvert p_r \rvert$	$\leq 0 \ \forall r \in [1,\infty]$	$\leq 0 \ \forall r \in [1,\infty]$	$\leq 0 \ \forall r \in [1,\infty]$	$\leq 0 \ \forall r \in [1,\infty]$	$\leq 0 \ \forall r \in [1,\infty]$
6	$\rho - \lvert p_t \rvert$	$\geq 0 \ \forall r \in [1,\infty]$	$\geq 0 \ \forall r \in [1,\infty]$	$\geq 0 \ \forall r \in [1,\infty]$	$\geq 0 \ \forall r \in [1,\infty]$	$\geq 0 \ \forall r \in [1,\infty]$
Model-2						
1	ρ	$\geq 0 \ \forall r \in [1,\infty]$	$\geq 0 \ \forall r \in [1,\infty]$	$\geq 0 \ \forall r \in [1,\infty]$	$\geq 0 \ \forall r \in [1,\infty]$	$\geq 0 \ \forall r \in [1,\infty]$
2	$\rho + p_r$	$\leq 0 \ \forall r \in [1,\infty]$	$\leq 0 \ \forall r \in [1,\infty]$	$\leq 0 \ \forall r \in [1,\infty]$	$\leq 0 \ \forall r \in [1,\infty]$	$\leq 0 \ \forall r \in [1,\infty]$
3	$\rho + p_t$	$\geq 0 \ \forall r \in [1,\infty]$	$\geq 0 \ \forall r \in [1,\infty]$	$\geq 0 \ \forall r \in [1,\infty]$	$\geq 0 \ \forall r \in [1,\infty]$	$\geq 0 \ \forall r \in [1,\infty]$
4	$\rho + p_r + 2p_t$	$\geq 0 \ \forall r \in [1,\infty]$	$\geq 0 \ \forall r \in [1,\infty]$	$\geq 0 \ \forall r \in [1,2.4) \leq 0 \ \forall r \in [2.4,\infty]$	$\geq 0 \ \forall r \in [1,1.8) \leq 0 \ \forall r \in [1.8,\infty]$	$\geq 0 \ \forall r \in [1,1.2) \leq 0 \ \forall r \in [1.2,\infty]$
5	$\rho - \lvert p_r \rvert$	$\leq 0 \ \forall r \in [1,\infty]$	$\leq 0 \ \forall r \in [1,\infty]$	$\leq 0 \ \forall r \in [1,\infty]$	$\leq 0 \ \forall r \in [1,\infty]$	$\leq 0 \ \forall r \in [1,\infty]$
6	$\rho - \lvert p_t \rvert$	$\leq 0 \ \forall r \in [1,\infty]$	$\leq 0 \ \forall r \in [1,\infty]$	$\leq 0 \ \forall r \in [1,\infty]$	$\leq 0 \ \forall r \in [1,\infty]$	$\leq 0 \ \forall r \in [1,\infty]$

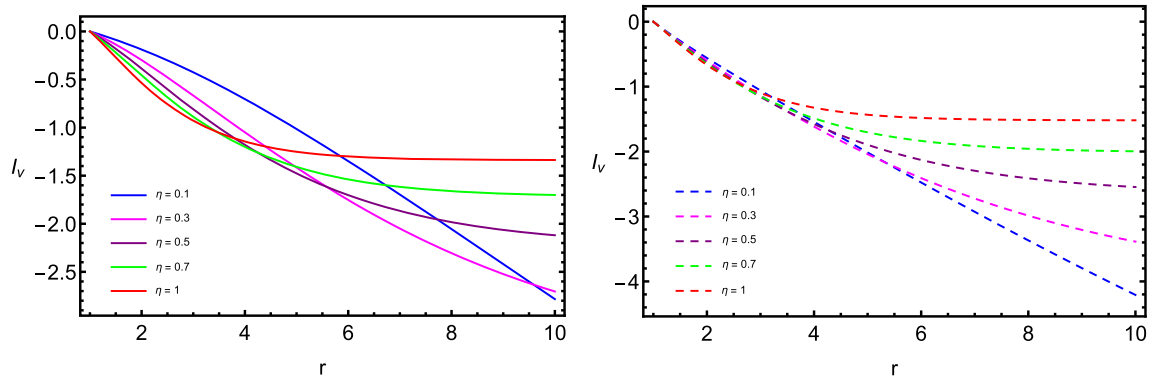

Fig. 12 Behavior of $\mathcal{I}_v$ against radial coordinate r for the case-I corresponding to the *Model-1* (left panel) and *Model-2* (right panel)

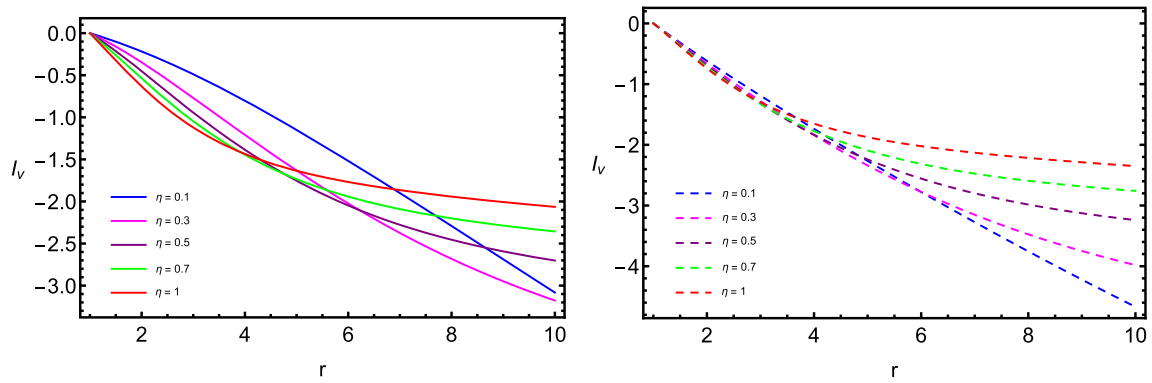

Fig. 13 Behavior of $\mathcal{I}_v$ against radial coordinate r for the case-II corresponding to the *Model-1* (left panel) and *Model-2* (right panel)

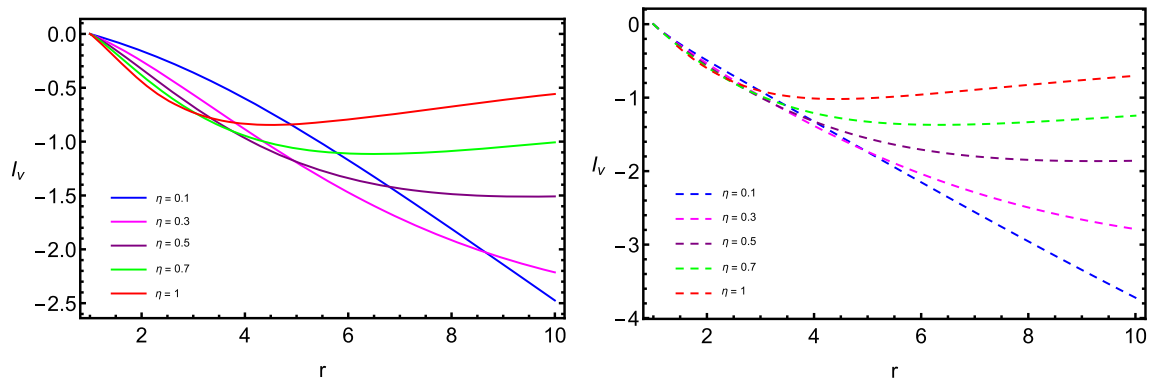

Fig. 14 Behavior of $\mathcal{I}_v$ against radial coordinate r for the case-III corresponding to the *Model-1* (left panel) and *Model-2* (right panel)

three-dimensional embedding diagrams in Figs. 3 and 14. The significant role of the parameter η for our wormhole configuration has been explored for five considered values like $\eta = 0.1, 0.3, 0.5, 0.7, 1$. Furthermore, an interesting fact that our wormhole configuration has been analyzed corresponding to three redshift functions $\Phi(r) = \text{constant} = K$, $\Phi(r) = \log\left(\frac{\xi}{r} + 1\right)$ and $\Phi(r) = e^{-\gamma/r}$, shortly named as Case-I, Case-II and Case-III respectively. And each of these three cases was analyzed by dividing into two models viz. *Model-1* corresponding to the general anisotropic EoS $p_t = \chi p_r$ and *Model-2* corresponding to the linear phantom-like EoS $p_r + \omega\rho = 0$. Importantly, for the judgement of NEC, WEC, SEC and DEC, we have drawn a large but sufficient no. of figures (Figs. 6, 7, 8, 9, 10, 11) for both models by considering the wormhole throat radius $r_0 = 1$. Also, for a better understanding of energy conditions, we have reported behaviors of ρ, $\rho + p_r$, $\rho + p_t$, $\rho + p_r + 2p_t$, $\rho - |p_r|$ and $\rho - |p_t|$ etc. w. r. t. radial coordinate r. near the wormhole throat in tabular forms like Tables 3, 4 and 5. Moreover, we have explored an essential discussion like ANEC regarding the minimum amount of exotic matter near the worm-

hole throat. Now some fruitful results of our whole study are reported below as follows:

From Figs. 3 and 4, we have confirmed that our proposed shape function (42) satisfied all necessary requirements to form the shape of a wormhole corresponding the respective throat radius $r_0 = 1$ and $r_0 = 2$. Because the conditions like Throat Condition, Flaring out condition, and Asymptotically flatness condition hold good for each of selected values $\eta = 0.1, 0.3, 0.5, 0.7, 1$. Also, in Fig. 5, we have included the plots of proper radial distance $l(r)$ from the throat to ∞ and the numerical values of $l(r)$ and embedding surface function $Z(r)$ at some radial distance r are reported in the Tables 1 and 2.

For the three cases, i.e., Case-I, II, III, the obtained results show that NEC, WEC, SEC, and DEC are not satisfied appropriately at the neighbourhood of the wormhole throat corresponding to both models. It is important to mention that the fundamental requirement for the formation of a traversable wormhole is fulfilled by the existence of matter that must be completely different from ordinary matter, the so-named as exotic matter. Again the presence of exotic matter may be confirmed by the violation of energy conditions, especially NEC. Therefore the requirements for the existence of a traversable wormhole corresponding to our proposed model are fulfilled as the energy conditions are not satisfied near the wormhole throat. Based on the figure profiles 12, 13 and 14, it is concluded that NEC is violated near the throat, and hence the proposed wormhole is supported by a small amount of exotic matter.

In the present work, we have delivered an accurate construction of gravitational field equations in F–R geometry. Also, we have achieved a detailed set of solutions in the analytic approach and visualized 2D and 3D diagrams of wormhole shape function (42). Finally, it is concluded, based on the overall study, that our proposed wormhole model is viable and realistic.

Acknowledgements KPD is thankful to UGC, Govt. of India, for providing Senior Research Fellowship (F.no. 16-6(DEC.2017)/2018 (NET/CSIR)).

Data Availability Statement This is wholly a theoretical work, and all of the corresponding results are constructed from the equations. We did not generate any new data during this study. So, there are no data associated with this article.

Funded by SCOAP^3. SCOAP^3 supports the goals of the International Year of Basic Sciences for Sustainable Development.

Appendix

Morris–Thorne traversable wormhole metric [40] has already been described in details by several authors [65–67]. Now, we want to represents Morris–Thorne wormhole metric in the context of Randers type Finslerian geometry i.e., Finsler–Randers (F–R) geometry. For this purpose, first we have studied the Refs. [15,16,18,22,23,26,27,71] and observed 'how cosmological models are developed based on the FRW cosmological metric. Motivated by these refs., we may write the Morris–Thorne wormhole metric in the context of F–R geometry i.e., may be called by Morris–Thorne–Finsler–Randers metric as

$$F(x, y) = \sqrt{g_{ij} y^i y^j} + u_\lambda y^\lambda, \tag{73}$$

where

$$g_{ij}(x) = \text{diag}\left[e^{2\Phi(r)}, -\frac{1}{1-\frac{b(r)}{r}}, -r^2, -r^2\sin^2\theta\right]. \tag{74}$$

Here $\Phi(r) \equiv$ the redshift function and $b(r) \equiv$ the shape function of the wormhole structure.

By using the relations, given in the Eq. (20) and imposing the conditions $u_0'' \approx 0$ and $u_0'^2 \approx 0$, we can obtain the non-vanishing components of the Ricci tensors ($L_{\mu\nu}$) corresponding to the above metric (73) as

$$\begin{aligned} L_{00} = \frac{e^{\Phi(r)}}{8r^2}\Big[&u_0'\left(-rb'(r) + 4r(r-b(r))\Phi'(r) - 3b(r) + 4r\right) \\ &-4e^{\Phi(r)}\Big(\Phi'(r)\Big(rb'(r) + 2r(b(r)-r)\Phi'(r) + 3b(r) - 4r\Big) \\ &+2r(b(r)-r)\Phi''(r)\Big)\Big], \end{aligned} \tag{75}$$

$$\begin{aligned} L_{11} = \frac{e^{-\Phi(r)}}{8r^2(b(r)-r)}\Big[&u_0' r\left(-5r\left(b'(r) + 4(r-b(r))\Phi'(r)\right)\right. \\ &-3b(r) + 8r) - 4e^{\Phi(r)}\Big(r\Big(b'(r)\left(r\Phi'(r) + 2\right) \\ &+2r(b(r)-r)\left(\Phi''(r) + \left(\Phi'(r)\right)^2\right) \\ &\left.-b(r)\Phi'(r)\Big) - 2b(r)\Big)\Big], \end{aligned} \tag{76}$$

$$\begin{aligned} L_{22} = \frac{1}{4}\Big[&u_0' e^{-\Phi(r)}\left(rb'(r) + 2r(r-b(r))\Phi'(r) + 6b(r) - 7r\right) \\ &+2\left(b'(r) + 2(b(r)-r)\Phi(r)' + \frac{b(r)}{r}\right)\Big], \end{aligned} \tag{77}$$

$$L_{33} = \sin^2\theta L_{22}, \tag{78}$$

Now, it is important to mention that Morris–Thorne wormhole metric is also a spherically symmetric metric. Thus, in the similar way of the construction of field equations (30)–(32), we can easily construct the non-trivial field equations corresponding to Morris–Thorne wormhole metric (36) in

Fisler–Randers geometry utilizing the Eqs. (29) and (25). Next after solving these field equations, we have written the system of Eqs. (39)–(41).

References

1. A.G. Riess et al., Supernova Search Team Collaboration, Astron. J. **116**, 1009 (1998)
2. S. Perlmutter et al., Supernava Cosmology Project Collaboration, Astrophys. J. **517**, 565 (1999)
3. C.L. Bennett et al., Astrophys. J. **148**(Suppl.), 1 (2003)
4. M. Betoule et al., SDSS Collaboration, Astron. Astrophys. **568**, A22 (2014)
5. P.A.R. Ade et al., Plank Collaboration, Astron. Astrophys. **571**, A16 (2014)
6. P.A.R. Ade et al., Plank Collaboration, Astron. Astrophys. **594**, A13 (2016)
7. A. Pais, *Subtle is the Lord: The Science and Life of Albert Einstein* (Oxford University Press, Oxford, 1982)
8. A. Lue et al., Phys. Rev. D **69**, 044005 (2004)
9. M. Kunz, D. Sapone, Phys. Rev. Lett. **98**, 121301 (2007)
10. S. Nojiri, S.D. Odintsov, Int. J. Geom. Methods Mod. Phys. **04**(01), 115–145 (2007)
11. E. Bertschinger, P. Zukin, Phys. Rev. D **78**, 024015 (2008)
12. G.S. Asanov, Aeq. Math. **24**(207), 229 (1982)
13. G.S. Asanov, Found. Phys. **13**(501), 527 (1983)
14. G.S. Asanov, *Finsler Geometry, Relativity and Gauge Theories* (Kluwer Academic Publishers Group, Holland, 1985)
15. P.C. Stavrinos, A.P. Kouretsis, M. Stathakopoulos, Gen. Relativ. Gravit. **40**(1403), 1425 (2008)
16. A.P. Kouretsis, M. Stathakopoulos, P.C. Stavrinos, Phys. Rev. D **79**, 104011 (2009)
17. A.P. Kouretsis, M. Stathakopoulos, P.C. Stavrinos, Phys. Rev. D **86**, 124025 (2012)
18. R. Chaubey, B. Tiwari, A. Shukla, M. Kumar, Proc. Natl. Inst. Sci. India (Pt. A Phys. Sci.) **89**(757), 768 (2019)
19. X. Li, Z. Chang, Phys. Rev. D **90**, 064049 (2014)
20. P.C. Stavrinos, S.I. Vacaru, Class. Quantum Gravity **30**, 055012 (2013)
21. Z. Chang, X. Li, Phys. Lett. B **663**(103), 106 (2008)
22. S. Basilakos, P.C. Stavrinos, Phys. Rev. D **87**, 043506 (2013)
23. S. Basilakos et al., Phys. Rev. D **88**, 123510 (2013)
24. A. Triantafyllopoulos et al., Eur. Phys. J. C **80**, Article number: 1200 (2020)
25. E. Kapsabelis et al., Eur. Phys. J. C **81**, Article number: 990 (2021)
26. R. Raushan, R. Chaubey, Eur. Phys. J. Plus **135**, 228 (2020)
27. G. Papagiannopoulos et al., Class. Quantum Gravity **34**, 225008 (2017)
28. G. Papagiannopoulos et al., Eur. Phys. J. C **80**, 816 (2020)
29. E. Kapsabelis et al., 9 Aug (2022). arXiv:2208.05063v1 [gr-qc]
30. X. Tang, C. Yu, Differ. Geom. Appl. **58**, 83–102 (2018)
31. P.C. Stavrinos, A. Maria, Int. J. Geom. Methods Mod. Phys. **15**(03), 1850039 (2018)
32. L. Flamm, Beiträge zur einsteinschen gravitationstheorie. Phys. Z. **17**, 448 (1916)
33. K. Schwarzschild, (Sitzbcr. Press. Akad. Wiss. Berlin, 1916), p. 189
34. H. Reissner, Über die Eigengravitation des elektrischen Feldes nach der Einsteinschen Theorie. Annalen der Physik. **50**, 106–120 (1916)
35. G. Nordstrom, On the energy of the gravitational field in Einstein's theory. Verhandl. Koninkl. Ned. Akad. Wetenschap. Afdel. Natuurk. **26**, 1201–1208 (1918)
36. A. Einstein, N. Rosen, The particle problem in the general theory of relativity. Phys. Rev. **48**(1), 73:77 (1935)
37. J.A. Wheeler, *Geometrodynamics* (Academic, New York, 1962)
38. S.W. Hawking, Wormholes in space-time. Phys. Rev. D **37**, 904 (1988)
39. R.W. Fuller, J.A. Wheeler, Causality and multiply connected space time. Phys. Rev. **128**(2), 919–929 (1962)
40. M.S. Morris, K.S. Thorne, Am. J. Phys. **56**, 395 (1988)
41. M. Visser, S. Kar, N. Dadhich, Traversable wormholes with arbitrarily small energy condition violations. Phys Rev Lett **90**, 201102 (2003)
42. M.S. Morris, K.S. Thorne, U. Yurtsever, Wormholes, time machines, and the weak energy condition. Phys. Rev. Lett. **61**, 1446 (1988)
43. D. Hochberg, M. Visser, General dynamic wormholes and violation of the null energy condition. (1999). arXiv:gr-qc/9901020
44. F.S.N. Lobo, Exotic solutions in general relativity: traversable wormholes and warp drive spacetimes. Class. Quantum Gravity Res. 1–78 (2008)
45. S. Kar, N. Dadhich, M. Visser, Quantifying energy condition violations in traversable wormholes. Pramana **63**, 859 (2004)
46. D. Ida, S. Hayward, How much negative energy does a wormhole need? Phys. Lett. A **260**, 17581 (1999)
47. C.J. Fewster, T.A. Roman, On wormholes with arbitrarily small quantities of exotic matter. Phys. Rev. D **72**, 044023 (2005)
48. P.K.F. Kuhfittig, More on wormholes supported by small amounts of exotic matter. Phys. Rev. D **73**, 084014 (2006)
49. F. Rahaman, M. Kalam, M. Sarker, K. Gayen, A theoretical construction of wormhole supported by phantom energy. Phys. Lett. B **633**, 1613 (2006)
50. M. Jamil, P.K.F. Kuhfittig, F. Rahaman, S.A. Rakib, Wormholes supported by polytropic phantom energy. Eur. Phys. J. C **67**, 51320 (2010)
51. D. Hochberg, M. Visser, Dynamic wormholes, antitrapped surfaces, and energy conditions. Phys. Rev. D **58**, 044021 (1998)
52. S.A. Hayward, Dynamic wormholes. Int. J. Mod. Phys. D **8**, 37382 (1999)
53. E. Teo, Rotating traversable wormholes. Phys. Rev. D **58**, 024014 (1998)
54. P.K.F. Kuhfittig, Axially symmetric rotating traversable wormholes. Phys. Rev. D **67**, 064015 (2003)
55. F. Rahaman, M. Kalam, M. Sarker, A. Ghosh, B. Raychaudhuri, Wormhole with varying cosmological constant. Gen. Relativ. Gravit. **39**, 145 (2007)
56. J.P.S. Lemos, F.S.N. Lobo, S. Quinet de Oliveira, Morris–Thorne wormholes with a cosmological constant. Phys. Rev. D **68**, 064004 (2003)
57. M. Cataldo, S. del Campo, P. Minning, P. Salgado, Evolving Lorentzian wormholes supported by phantom matter and cosmological constant. Phys. Rev. D **79**, 024005 (2009)
58. F.S.N. Lobo, Phantom energy traversable wormholes. Phys. Rev. D **71**, 084011 (2005)
59. F.S.N. Lobo, Stability of phantom wormholes. Phys. Rev. D **71**, 124022 (2005)
60. O.B. Zaslavskii, Exactly solvable model of wormhole supported by phantom energy. Phys. Rev. D **72**, 061303 (2005)
61. S. Chakraborty, T. Bandyopadhyay, Modified Chaplygin traversable wormholes. Int. J. Mod. Phys. D **18**, 463 (2009)
62. M. Jamil, U. Farooq, M.A. Rashid, Wormholes supported by phantom-like modified Chaplygin gas. Eur. Phys. J. C **59**, 907 (2009)
63. P.K.F. Kuhfittig, A Single model of traversable wormholes supported by generalized phantom energy or Chaplygin gas. Gen. Relativ. Gravit. **41**, 1485 (2009)
64. D. Bao, S.S. Chern, Z. Shen, *An Introduction to Riemann Finsler Geometry* (Springer, New York, 2000)

65. F. Rahman, N. Paul, A. Banerjee, S.S. De, S. Ray, A.A. Usmani, The Finslerian wormhole models. Eur. Phys. J. C **76**, 246 (2016)
66. M. Malligawad et al., 6 Feb (2023). arXiv:2302.02983v1 [gr-qc]
67. B.R. Yashwanth et al., 23 Feb (2023). arXiv:2302.09788v2 [gr-qc]
68. K.N. Singh et al., Traversable Finslerian wormholes supported by phantom energy. Front. Phys. **10**, 1038905 (2023)
69. G. Randers, Phys. Rev. **59**, 195 (1941)
70. H. Rund, *The Differential Geometry of Finsler Spaces* (Springer, Berlin, 1959)
71. P.C. Stavrinos, F.I. Diakogiannis, Gravit. Cosmol. **10**(4), 1 (2005)
72. F.S.N. Lobo, *Wormholes, Warp Drives and Energy Conditions* (Springer, Berlin, 2017)
73. B. Ghosh, S. Mitra, Int. J. Mod. Phys. A **36**(18), 2150119 (2021)
74. S.V. Sushkov, S.M. Kozyrev, Composite vacuum Brans–Dicke wormholes. Phys. Rev. D **84**, 124026 (2011)
75. S.W. Hawking, G.F.R. Ellis, *The Large Scale Structure of Space-Time* (Cambridge University Press, Cambridge, 1973)
76. M. Visser, *Lorentzian Wormholes: From Einstein to Hawking* (AIP Press, Springer, New York, 1996)
77. M. Novello, J.M. Salim, Phys. Rev. D **20**, 377 (1979)
78. M. Novello, L.A.R. Oliveira, J.M. Salim, E. Albaz, Int. J. Mod. Phys. D **1**, 641 (1993)
79. P. Peter, N. Pinto-Neto, Phys. Rev. D **65**, 023513 (2002)
80. V.A. De Lorenci, R. Klippert, M. Novello, J.M. Salim, Phys. Rev. D **65**, 063501 (2002)
81. T. Singh, R. Chaubey, A. Singh, Eur. Phys. J. Plus **130**, 31 (2015)
82. G. Date, (2007). arXiv:0704.0145 [gr-qc]
83. N. Pinto-Neto, F.P. Poulis, J.M. Salim, Int. J. Mod. Phys. A **24**(20n21), 4009–4020 (2009)
84. P. Pavlović, M. Sossich, Eur. Phys. J. C **83**, Article number: 235 (2023)
85. S. Halder et al., Phys. Lett. B **791**, 270–275 (2019)